Materials for Renewable and Sustainable Energy (2024) 13:133–153
https://doi.org/10.1007/s40243-024-00255-w

REVIEW PAPER

Desirable candidates for high-performance lead-free organic–inorganic halide perovskite solar cells

Sajid Sajid[1,2,3] · Salem Alzahmi[1,2] · Imen Ben Salem[3] · Nouar Tabet[4] · Yousef Haik[5,6] · Ihab M. Obaidat[4]

Received: 14 November 2023 / Accepted: 4 January 2024 / Published online: 16 February 2024

Abstract

Perovskite solar cells (PSCs) are currently demonstrating tremendous potential in terms of straightforward processing, a plentiful supply of materials, and easy architectural integration, as well as high power conversion efficiency (PCE). However, the elemental composition of the widely utilized organic–inorganic halide perovskites (OIHPs) contains the hazardous lead (Pb). The presence of Pb in the PSCs is problematic because of its toxicity which may slow down or even impede the pace of commercialization. As a backup option, the scientific community has been looking for non-toxic/less-toxic elements that can replace Pb in OIHPs. Despite not yet matching the impressive results of Pb-containing OIHPs, the community is paying close attention to Pb-free materials and has seen some encouraging findings. This review evaluates the Pb-replacement with suitable elements and scrutinizes the desirable optoelectronic features of such elements in OIHPs. The fundamental features of Pb-free OIHPs together with their photovoltaic performance in the PSCs are evaluated in details. Finally, we sum up the current challenges and potential opportunities for the Pb-free OIHPs and their devices.

Keywords Lead-free · Non-toxic · Perovskite · Optoelectronic feature · Performance

Introduction

The commonly utilized lead (Pb)-based organic–inorganic halide perovskites (OIHPs) have a number of desirable features, including a broad absorption spectrum, a long diffusion length, a low exciton binding energy, and excellent charge-carrier mobility [1]. The power conversion efficiency (PCEs) of perovskite solar cells (PSCs) using Pb-containing OIHPs as photoactive materials increased dramatically, from 3.8% to 26% [2]. The Pb-based PSCs are showing significant promise for future applications as they evolve toward high efficiency and better stability [3–5]. The intrinsic toxicity of Pb-based perovskites, however, is a critical challenge for both humans and environment [6, 7]. According to research, Pb poisoning of soil and water supplies has a very substantial adverse effect on the life of people, animals, and plants [8, 9]. In general, Pb intake of up to 0.5 mg/day causes the majority of people to exhibit Pb poisoning symptoms [10, 11]. The most commonly perovskite material currently used in PSCs is methyl ammonium lead iodide ($CH_3NH_3PbI_3$). The absorbing layer has a typical thickness of 500 nm. This corresponds to a Pb content of 0.6 g/m^2. It is worth noting that this is lower than the Pb content of a typical conventional silicon PV panel which is about 6 g/m^2 [12]. However, dynamic leaching tests showed that the leaching concentration of Pb from PSCs could exceed the hazardous waste limit of 5 mg/L [13].

In order to prevent Pb leakage from Pb-based PSCs, a number of encapsulation approaches are currently being applied. These methods involve capturing Pb through

✉ Salem Alzahmi
iobaidat@sharjah.ac.ae

✉ Ihab M. Obaidat
s.alzahmi@uaeu.ac.ae

1 Department of Chemical & Petroleum Engineering, United Arab Emirates University, P.O. Box 15551, Al Ain, United Arab Emirates

2 National Water and Energy Center, United Arab Emirates University, P.O. Box 15551, Al Ain, United Arab Emirates

3 College of Natural and Health Sciences, Zayed University, P.O. Box 144534, Abu Dhabi, United Arab Emirates

4 Department of Applied Physics and Astronomy, University of Sharjah, P.O. Box 27272, Sharjah, United Arab Emirates

5 Department of Mechanical and Nuclear Engineering, University of Sharjah, Sharjah, United Arab Emirates

6 Department of Mechanical Engineering, The University of Jordan, Amman, Jordan

cation-exchange resins or functionalized metal–organic structures, reducing Pb diffusion using an epoxy resin with a natural healing function, and sequestering Pb using a protective covering of Pb-absorbing material [14–17]. However, these attempts have not completely wiped out the risks for Pb toxicity. In this context, replacing the Pb in PSCs is crucial for developing affordable clean energy conversion technology that will help humanity in the long run. Divalent and trivalent elements, such as Sn^{2+}, Ge^{2+}, Cu^{2+}, Bi^{3+}, and Sb^{3+}, among others, have received a lot of focus recently due to their distinctive optoelectronic properties and have been widely explored as potential eco-friendly replacements for hazardous Pb^{2+} [18–24]. From a basic standpoint, Pb-free OIHPs-based PSCs have great optoelectronic properties and high theoretical efficiency [25], so why do their PCEs trail those of Pb-based equivalents by such a large margin? The following explanations are given as the accepted reasons, including the rapid oxidation of metal ions, undesirable composition and inferior thin-films morphologies [26, 27]. Consequently, these issues need to be resolved in order to enhance the performance and durability of Pb-free PSCs.

In this review, we first discuss the optoelectronic properties of Pb-free OIHPs. The following sections offer an in-depth examination of methods for reducing metal ion oxidation and enhancing the performance and stability of Pb-free PSCs, including the optimization of composition and grain boundaries (GBs), in light of recent studies on Pb-free OIHPs. We present our own viewpoints on the potential advancement of Pb-free PSCs in the last section.

Optoelectronic features

Before replacing Pb in OIHPs, some of the fundamental features of the alternative elements are mandatory to discuss, such as crystal structure, energy bandgap, and charge carriers density. In this section, we will scrutinize these features and their importance in the Pb-free OIHPs.

Crystal structure

According to Fig. 1, the general formula for organic–inorganic trihalide perovskite is ABX_3, where A is a cation, B is a cation, and X is a halogen anion [28]. The halogen anion often consists of Cl, Br, I, or their mixture, while the cation typically consists of methylammonium (MA), formamidinium (FA), Cs, Rb, or their mixture. It has been demonstrated in the earlier research that B cations, such as Pb^{2+}, can be substituted with less harmful ions like Cu^{2+}, Sn^{2+}, Ge^{2+}, Bi^{3+}, and Sb^{3+} [29–34]. Such cations were added, which not only broadens the range of perovskite species but also improves PSC's environmental friendliness. Additionally, it has been demonstrated that the ABX_3-perovskite's physical and electrical properties are determined by structure distortions [35]. For the dimensional assessment of a perovskite, for instance, the following Eq. (1) can be used:

$$t = \frac{(r_A + r_X)}{\sqrt{2}(r_B + r_X)} \tag{1}$$

where t, r_A, r_B and r_X denote the Goldschmidt's tolerance, and ionic radii of A, B and X, respectively. A high-symmetry cubic three-dimensional (3D) perovskite is generated if the value of "t" falls within the range of 0.813 and 1.107, whereas other values of "t" result in the formation of two-dimensional (2D), one-dimensional (1D), and

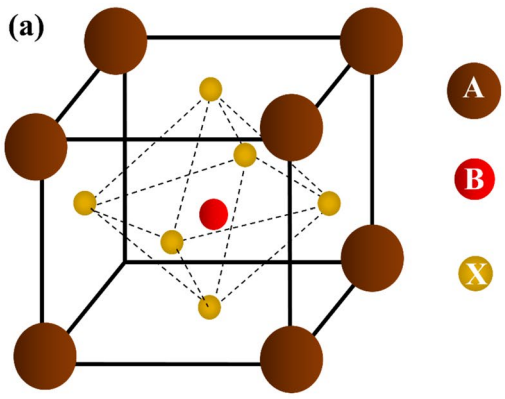

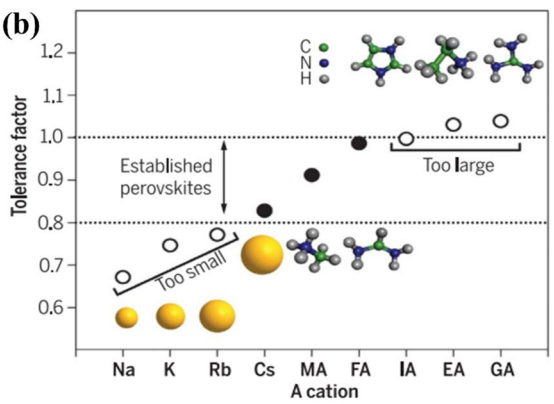

Fig. 1 **a** Basic crystal structure of perovskites, where A represent: MA^+ ($CH_3NH_3^+$) or FA^+ ($CH(NH_2)_2^+$) or Cs^+ etc., B represent: Cu^{2+}, Pb^{2+}, Sn^{2+}, Ge^{2+}, Bi^{3+}, Sb^{3+} etc., and X represent: I^-, Cl^-, Br^-. **b** Tolerance factor for A-site cations with various ionic radii in ABX_3 perovskites. Reproduced with permission [39]. Copyright 2017, American Association for the Advancement of Science (AAAS)

zero-dimensional (0D) perovskites [36, 37]. Because the kinetics of charges are affected by the structural dimensionality of the OIHPs, it is thought to be one of the most important aspects. However, this assessment is insufficient to be used for all OIHPs. The probe for electronic dimensionality is therefore equally crucial [38]. For instance, due to the barrier to isotropic current flow, the large effective masses of holes/electrons, and the deeper defect states, the OIHPs with low electronic dimensionality but high structural dimensionality have fewer promising applications as photoactive materials.

By categorizing them according to their crystal structures, OIHPs exhibit distinct charge transport characteristics due to their structural make-up and dimensionality. The optical energy bandgap can be adjusted by altering the compositions of A, B, or X in the ABX_3 perovskites. Although the organic cation-A can cause geometrical distortions in the inorganic layers, which modify the bandgap, it does not directly contribute to the bandgap in the same way as B and X do. For instance, the symmetry changes from tetragonal to cubic when the size of A shrinks [40], often causing a reduction in the bandgap. Modifications to X have a direct effect on the bandgap because they alter the size of the unit cell. The bandgap widens as the halide's size shrinks. According to the Shockley–Queisser limit [41], the optical bandgaps of Pb-based perovskites deviate from the ideal bandgap of a single junction solar cell (1.34 eV); thus, Pb substitutions may provide better bandgaps for conversion of solar energy. For example, the bandgap of $MASn_{1-x}PbxI_3$ can be regulated between 1.17 and 1.55 eV, allowing perovskites to absorb light from the visible spectrum to the infrared region [42]. A 3D perovskite that is a member of the pseudo-cubic *Pm3m* space group is $MASnI_3$. This structure is composed of units of $[BX_6]^{4+}$ octahedral in a 3D network, with A^+ residing in the space between the neighboring octahedral. In parent 3D perovskite structure's third B-site can be eliminated to create 2D layer phase. By increasing the number of octahedral sheets from $n=1$ to $n=\infty$, the bandgap of 2D perovskite $(BA)_2(MA)_{n-1}Sn_nI_{3n+1}$ may be controlled from 1.83 eV to 1.20 eV [43]. Due to their tight packing and higher formation energy, 2D perovskites have demonstrated a higher moisture stability, providing new methods to stabilize PSCs [44]. To concurrently increase efficiency and stability for PSCs, efforts have been made to mix 3D perovskites with 2D perovskites in addition to stand-alone 2D perovskites [45] as shown in Fig. 2.

It is desirable to look for elements in the quest to replace toxic Pb in the OIHPs; the suggested elements include tin (Sn), bismuth (Bi), germanium (Ge), antimony (Sb), and copper (Cu). The ideal perovskite layers for Pb-free PSCs will have low toxicity, low direct bandgaps, high optical absorption coefficients, high carrier mobilities, low exciton-binding energies, long charge-carrier lifetimes, and suitable stability. Alternatives to perovskites made without Pb should be inexpensive, abundant, recyclable, and capable of reforming into stable perovskite structures. Furthermore, for them

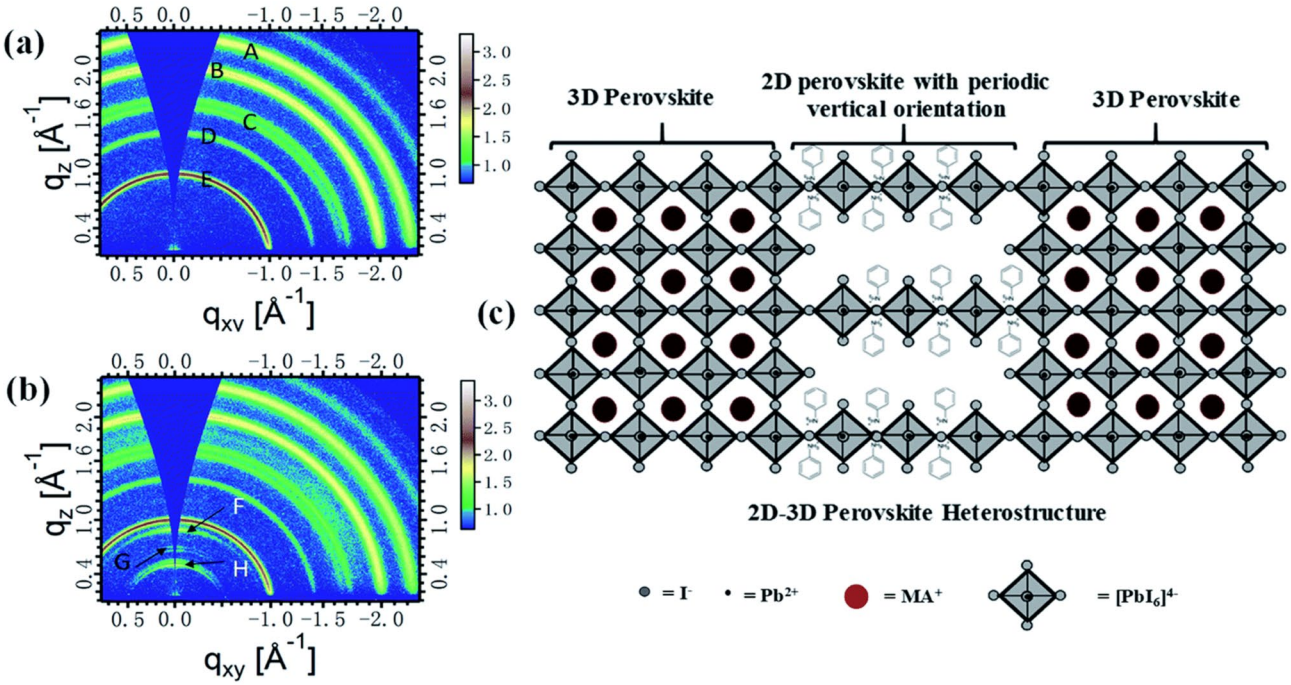

Fig. 2 **a**, **b** Grazing-incidence wide-angle X-ray scattering (GIWAXS) images of the 3D and 2D/3D perovskites, respectively. **c** Schematic illustration of the 2D/3D perovskite heterojunction. Reproduced with permission [45]. Copyright 2020, Royal Society of Chemistry

to be competitive, they must meet commercial demands for efficiency, adaptability, and stability and be able to be processed cheaply at scale employing solution-processed technologies.

Energy band structure

Since the energy bandgap is the first factor to be consider for Pb-free OIHPs in order to harvest the suitable range of light, it is crucial to analyze the energy bandgap of the absorbing material before considering its use in the PSCs. Theoretically, density functional theory is a widely used tool to determine the energy bandgap and band structures of the OIHPs. For example, antibonding between the orbitals of Sn-5 s and I-5p display the valence band maximum (VBM) of $MASnI_3$, whereas the conduction band maximum (CBM) is mainly due to Sn-5p orbital [30–32]. In addition, the Sn-based OIHPs mostly have smaller energy bandgaps compared to the Pb-based OIHPs, which makes them suitable to harvest more light. Spin–orbit coupling method demonstrates the similar CBM dispersion in $MASnI_3$ and $MAPbI_3$, while $MASnI_3$ shows larger VBM dispersion, demonstrating lower effective masses and smaller binding energies of the charge-carriers [46]. This shows that the Sn-based OIHPs mostly possess low energy bandgaps as compared to the Pb-based OIHPs. The relatively low energy bandgap of the Sn-based OIHPs can be attributed to the weak binding between Sn s and I p orbitals than that of Pb and I orbitals [33]. This means that the band edges of $MASnI_3$ are less strongly bonded compared to the $MAPbI_3$, which results in small bandgap of the Sn-based OIHPs. It has been suggested previously that the A-cations can indirectly modify the bandgaps of both Pb-based and Pb-free perovskites. The corner-sharing octahedral distortion may be the reason behind this effect. As reported in $FAPbI_3$ (1.48 eV), $MAPbI_3$ (1.53 eV), and $CsPbI_3$ (1.53 eV), A-cation with a small radius is likely to increase the bandgaps of the Pb-based perovskite [47]. However, the bandgaps of Pb-free perovskites like $FASnI_3$ (1.41 eV) [48], $MASnI_3$ (1.30 eV) [49], and $CsSnI_3$ (1.25 eV) [50] are reduced by the insertion of A-cations with smaller radii, as depicted in Fig. 3a [33]. Different A-cations cause the perovskite lattice to deform in

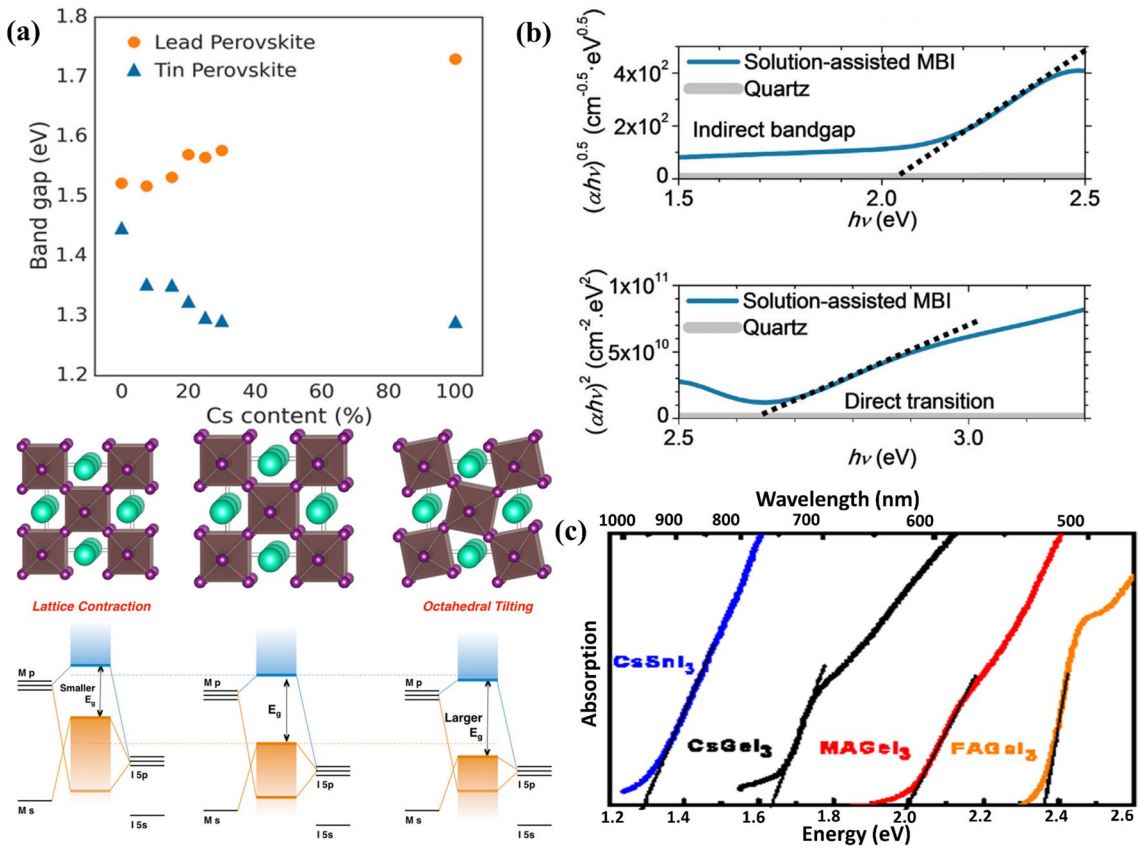

Fig. 3 **a** Optical bandgap of $FA_{1-x}Cs_xSnI_3/FA_{1-x}Cs_xSnI_3$ as a function of Cs content accompanied by schematic illustration of perovskite lattice and energy level diagrams. Reproduced with permission [33]. Copyright 2017, American Chemical Society. **b** Indirect bandgap and higher energy transition in MBI. Reproduced with permission [51]. Copyright 2016, WILEY–VCH Verlag. **c** Optical absorption spectrum of $CsGeI_3$, $MAGeI_3$ and $FAGeI_3$, in comparison with $CsSnI_3$. Reproduced with permission [52]. Copyright 2015, Royal Society of Chemistry

various ways. For Pb-based perovskites, as the cation radius decreases, $[PbI_6]^{4-}$ octahedra are tilted with smaller Pb-I-Pb bond angles, resulting in reduced orbital overlap between Pb and I, shifting the valence band to deeper energy levels, and thereby increasing the bandgap; however, for Sn-based perovskites, because Sn^{2+} is smaller than Pb^{2+}, it is simply contracted [33].

Substituting Pb/Sn with bismuth, methylammonium bismuth iodide $(CH_3NH_3)_3Bi_2I_9$ (MBI) can be a suitable candidate to replace methylammonium Pb/Sn iodide. MBI is made up of two face-sharing (bismuth iodide octahedral), which exhibits certain appealing characteristics like low-temperature phase transitions, dielectric properties, and optical properties [53–55]. For instance, the absorption spectrum revealed that MBI has two absorption onsets (Fig. 3b), a bandgap of 2.04 eV [51], and a substantial optical absorption coefficient (10^5 cm^{-1} in the visible-light Range) above 1.1 eV, which is ideally suited for the top cell of a tandem device. When compared to Pb-based devices, the MBI-based PSCs have demonstrated better stability [56]. However, the MBI-based PSCs had very poor photovoltaic performance due to the broad optical bandgap (2.1–2.4 eV), indirect gap, and substantial defect states [57]. According to Hebig et al. [58], the bandgap of $(CH_3NH_3)_3Sb_2I_9$ is approximately 2.14 eV, and it has high absorption coefficients in the range of greater than 10^5 cm^{-1}, making it ideal for efficient light absorption in thin-film photovoltaic. Additionally, compared to $Cs_3Bi_2I_9$, $MA_3Bi_2I_9$, and $FA_3Bi_2I_9$, the Sb-based perovskite had lower sub-bandgap absorption, indicating a lower density of defect states compared to the Bi-perovskites. The bandgap can be decreased in the Sb-based perovskite. For instance, according to Boopathi et al. [59], the optical bandgaps of SbI_3, $MA_3Sb_2I_9$, HI-$MA_3Sb_2I_9$, $Cs_3Sb_2I_9$, and HI-$Cs_3Sb_2I_9$ are 2.60, 2.20, 1.95, 2.30, and 2 eV, respectively. Due to phase purity and crystallinity, the addition of hydroiodic acid (HI) decreased the bandgaps in both Sb-based perovskites (HI-$MA_3Sb_2I_9$ and HI-$Cs_3Sb_2I_9$), which is beneficial for absorption in the higher wavelength region.

Ge is another potential replacement for Pb. By creating a series of Ge-based perovskites using various cations, for instance, Stoumpos et al. first suggested the potential of Ge-based perovskites [19]. It was noticed that the Ge-based perovskites had an energy bandgap range of 1.60 to 3.80 eV and crystallize in a trigonal crystal structure. Different cations can affect the bandgap of the Ge-based perovskite, as seen in Fig. 3c [52]. Ge-based perovskites could be suitable for achieving high open circuit voltage (V_{oc}) even though they have bandgaps that are larger than the ideal one predicted by the Shockley–Queisser limit. Some reports suggested a mixed metal-cations technique to further decrease the bandgap of Ge-based perovskites [60]. For instance, the OIHPs based on combined Sn and Ge with bandgaps of 1.4–1.5 eV are appropriate for PSCs applications [61].

Researchers also continued to look at Cu as a potential replacement for Pb. According to Cui et al. [62], the optical bandgaps are 1.74 eV for (p-F-$C_6H_5C_2H_4$-NH_3)-$CuBr_4$ and 1.76 eV for $(CH_3(CH_2)_3NH_3)_2$-$CuBr_4$, estimated from the film absorption onsets. Figure 4a, b show excellent optical absorption over the whole visible spectrum for anions mixing in Cu-based perovskites like $C_6H_4NH_2CuBr_2I$, which also has a direct energy bandgap of 1.64 eV [63]. At 450 nm, $C_6H_4NH_2CuBr_2I$ has an absorption coefficient of about 0.6×10^5 cm^{-1}, which is high enough to efficiently absorb light. 2D-$(C_6H_5CH_2NH_3)_2CuBr_4$ displays energy bandgap of 1.81 eV and high absorption coefficient of 1×10^5 cm^{-1} at the most intense absorption at 539 nm [20], indicating that it is excellent for light-harvesting. Furthermore, Cu-based perovskites with the general formula $(CH_3NH_3)_2CuX$, where X is Cl_4, Cl_2I_2, or Cl_2Br_2, have been synthesized, and studied for Pb-free PSCs [64]. Additionally, by varying the Cl/I/Br content ratio, it is possible to tune optical absorption in the wavelength of 300–900 nm range, or visible to near-infrared range, as well as direct bandgaps from 1.04 eV to 2.36 eV, as depicted in Fig. 4**c**, **d**.

Charge-carriers density and type

The charge-carrier densities in OIHPs can vary depending on several factors, including the specific type of perovskite, the fabrication method, and the environmental conditions. OIHPs can have relatively high charge-carrier densities. The intrinsic charge-carrier density is primarily determined by the bandgap and temperature. At room temperature, typical intrinsic charge-carrier densities in the range of 10^{14} to 10^{17} cm^{-3} are common for many perovskites. Charge-carrier densities can be modified through doping. By introducing certain types of dopants (e.g., n-type or p-type), it is possible to significantly alter the charge-carrier concentration. Doping can be used to enhance the electrical conductivity and tailor the material's properties for specific applications. The charge-carrier densities in OIHPs can also be influenced by the presence of defects and trap states within the crystal lattice. These defects can capture and immobilize charge carriers, reducing the effective charge-carrier density and impacting the material's performance. The charge-carrier densities of 10^{18} cm^{-3} [26, 65] for pure Sn-based perovskites are higher than those of Pb counterparts (10^{15}–10^{16} cm^{-3}) [66]. Sn-based perovskites act as p-type with high background carrier densities, which is primarily due to quick oxidation of Sn^{2+} to Sn^{4+} and inherently generated Sn vacancies [67]. An excessively high carrier densities would compromise the PSCs performance since it would shorten the carrier diffusion length [26], as shown in Fig. 5a. The fact that the exciton binding energies (26 meV) in Sn-based perovskites are in the same range as those in Pb counterparts (2–50 meV) suggests that exciton dissociation occurs easily

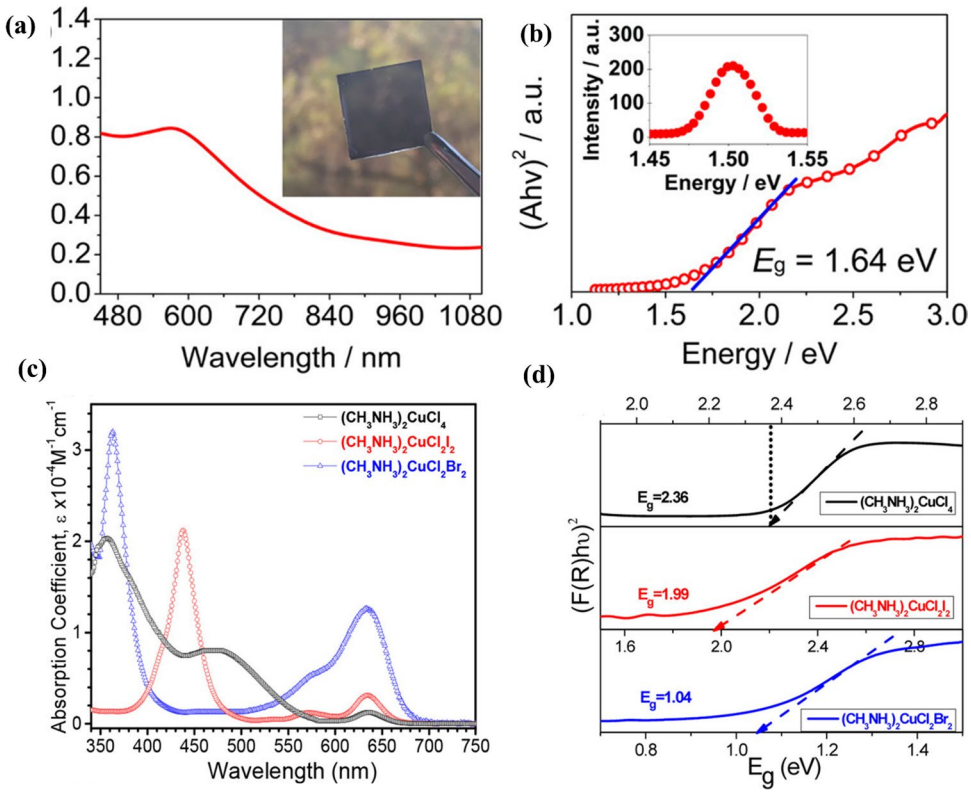

Fig. 4 **a** UV–Vis spectra of $C_6H_4NH_2CuBr_2I$ layer (inset is the photograph). **b** Energy bandgap and photoluminescence spectra of the $C_6H_4NH_2CuBr_2I$. Reproduced with permission [63]. Copyright 2017, American Chemical Society. **c**, **d** Absorption coefficient and FT-IR spectra of the $(CH_3NH_3)_2CuCl_4$, $(CH_3NH_3)_2CuCl_2I_2$, and $(CH_3NH_3)_2CuCl_2Br_2$. Reproduced with permission [64]. Copyright 2018, American Chemical Society

at room temperature and does not restrict the formation of free carriers [66]. Small effective masses of the charge-carriers in Sn-based perovskites could be the reason of low binding energies of excitons, which in turn may be brought on by the high dispersion of valence and conduction bands [68].

The average conductivity and resistivity for the $CH_3NH_3)_3Bi_2I_3$ (MBI) films are reported to be 0.0083 S cm^{-1} and 121.04 Ω cm [56]. The Hall-Effect measurement for the MBI films revealed that the Hall coefficients are positive, confirming the carrier's (p-type) positive sign. The MBI film's predicted carrier concentration of 10^{16} cm^{-3}, which is comparable to SnF_2-doped $CsSnI_3$ (10^{17} cm^{-3}) and significantly less than that of pristine $CsSnI_3$ (10^{19} cm^{-3}) [69, 70]. However, according to Miaoqiang et al. [56], the intrinsic carrier concentration of the MBI (10^9 cm^{-3}) is substantially higher than that of $MAPbI_3$. The perovskite layer's high background carrier densities may promote bulk recombination, which could lower the solar cell's V_{oc}. The reported V_{oc} is significantly lower than that of planar MBI film-based solar cells (0.510 V), being just 0.01 V for the pure $CsSnI_3$ and 0.24 V for $CsSnI_3$ that has been doped with SnF_2 [56, 69]. Such a V_{oc} trend is in line with the background carrier densities, indicating that lowering the background carrier concentration may offer a further way of improving the performance of MBI-based solar cells. In comparison to $MASnI_3$ (2320 cm^2 V^{-1} s^{-1}) and p-type $CsSnI_3$ (520 cm^2 V^{-1} s^{-1}), the carrier mobility of the MBI film is around 1 cm^2 V^{-1} s^{-1} [71]. Additionally, Fig. 5b describes the use of space charge limited conduction to determine the charge carrier's mobilities in MBI [72]. For a hybrid organic/inorganic material, the MBI has a mobility of 29.7 cm^2 V^{-1} s^{-1}, which is comparable to the $MAPbI_3$ mobility of 38 cm^2 V^{-1} s^{-1} [73]. The relatively poor performance of MBI-based solar cells may be a result of the low carrier mobility in the MBI layer. Doping, which has been shown to be extremely effective in $CsSnI_3$, may provide a way to control carrier concentration and carrier mobility and so further enhance the device performance of MBI film-based devices [69]. The carrier dynamics deficit and poor solar performance are primarily attributable to the concentration of trap states inside perovskites or related interfaces. To understand the effects of Ge addition in passivating and lowering trap states thermally stimulated current was used by some reports, as shown in Fig. 5c, d [74, 75]. When Ge is added to $FA_{0.75}MA_{0.25}Sn_{1-x}Ge_xI_3$, the trap density is dramatically reduced from 10^{15}–10^{17} cm^{-3} (without Ge) to 10^8–10^{14} cm^{-3}, resulting in longer charge diffusion lengths (1 μ m) and lifetimes, as well as high charge mobility and a 7.9% efficiency. Fascinatingly, the trap density profile of the $FA_{0.75}MA_{0.25}Sn_{1-x}Ge_xI_3$ is identical to that of the $MAPbI_3$, and it has a long charge diffusion length. Perovskites based on Sb have comparable charge-carrier mobilities as well. For instance, a single crystal of $(NH_4)_3Sb_2I_9$ demonstrates 4.8 cm^2 V^{-1} s^{-1} hole mobility and 12.3 cm^2 V^{-1} s^{-1} electron

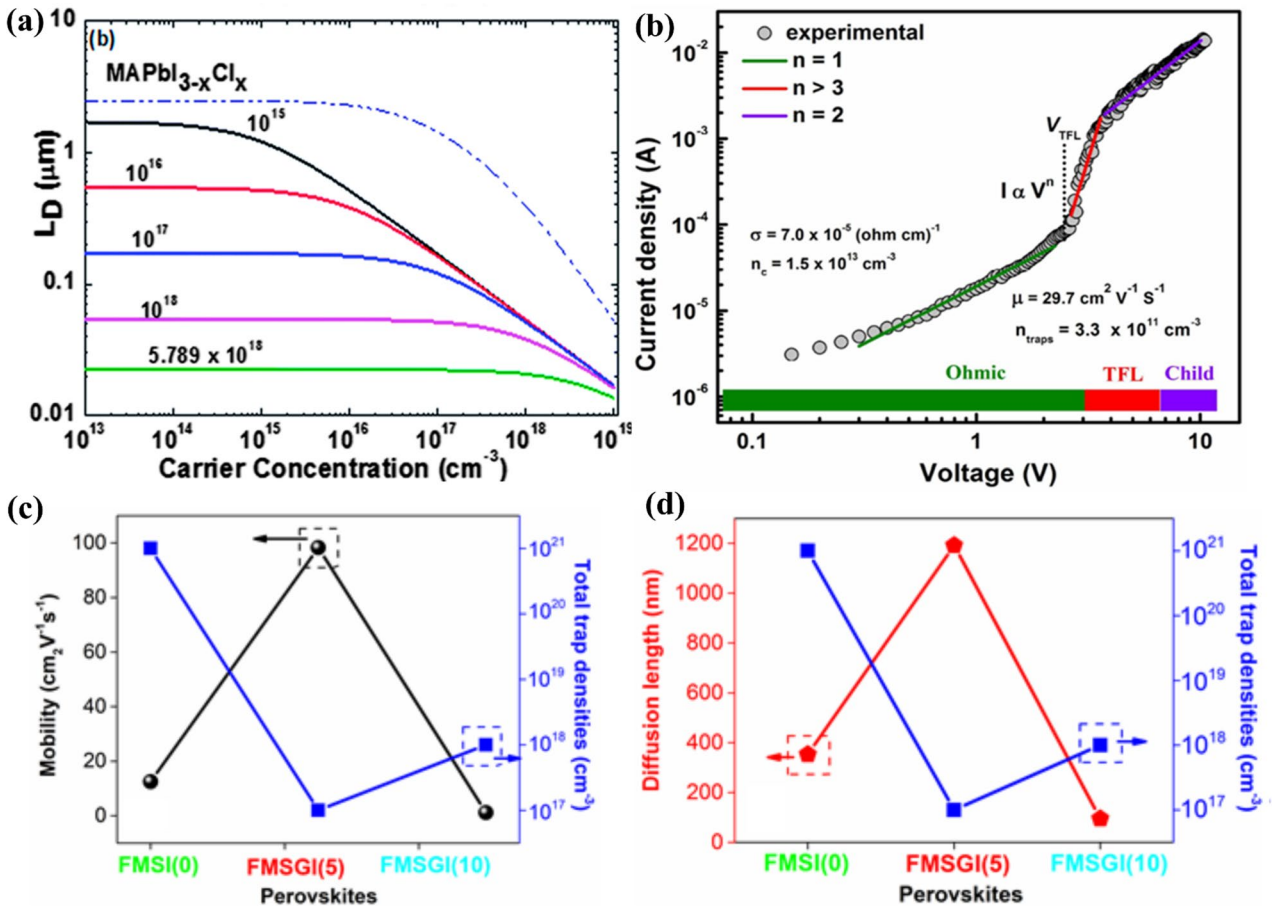

Fig. 5 **a** Diffusion length (L_D) against the carrier concentration for different hole doping levels. Reproduced with permission [26]. Copyright 2014, Royal Society of Chemistry. **b** Current to voltage curve of the ITO/$(CH_3NH_3)_3Bi_2I_9$/Au device. Reproduced with permission [72]. Copyright 2016, Royal Society of Chemistry. **c**, **d** Mobility and diffusion length versus total trap densities of $FA_{0.75}MA_{0.25}Sn_{1-x}Ge_xI_3$ ($FMS_{1-x}G_xI$) at various Ge concentrations. Reproduced with permission [74]. Copyright 2019, Elsevier Ltd

mobility [76]. The Cu-based perovskites generally display n-type nature with electron mobilities ranges from 19.84 to 22.16 $cm^2\ V^{-1}\ s^{-1}$ [24, 63].

Challenges of Pb-free OIHPs

Thin-films of the Pb-free perovskites must be of the best quality to produce efficient and long-lasting PSCs. The procedure and the duration of the subsequent treatment, the substrate on which the perovskites are fabricated, the quality and age of the chemicals used, the solvents' coordinating strength and boiling point, the ambient conditions of the processing environment, and many other factors are some of the variables that impact the thin-film quality and afterwards optoelectronic features of the resulting perovskites. The Pb-free perovskites showed nearly identical electrical and optical properties to Pb-based OIHPs. However, the PCEs are still much lower than Pb-based devices. For example, compared to Pb-based PSCs, the maximum PCE based on pure Sn-based PSCs is much lower at 14.81% [77]. For instance, in the case of Sn-based perovskites, the following could be the primary causes of the Pb-free PSC's inferior performance: There are several factors that make it difficult to obtain high performance, including: (1) fast oxidation of Sn^{2+} to Sn^{4+} even in the presence of little moisture and oxygen in the glovebox [78]; (2) low formation energy of Sn vacancies that result in p-type self-doping [18, 26]; (3) uncontrollable crystallization due to the rapid reaction between inorganic and organic salts [79]; and (4) undesirable frontier energy level alignment that results in energy barriers at the corresponding interfaces with charge transport layers. Other Pb-free perovskites almost certainly suffer from the same problems, which lead to low efficiency and instability in Pb-free PSCs. The performance development and methods to improve device performance will be covered in details in the following discussion.

Strategies for improving Pb-free OIHPs performance

Compositional engineering

The majority of the high performance Pb-free-based PSCs are reported with mixed cations and anions. Similar to Pb-based PSCs, compositional engineering is an effective approach for controlling the crystal structure, bandgap, and stability of Pb-free-based perovskites under stressful conditions (such as light, heat, and moisture). Additionally, low cation-vacancy formation energy is caused by the undesirable *s-p* antibonding coupling in cation–anion bonds; however, compositional engineering can lower self-doping and trap-state concentrations [80]. The effect on the performance of Pb-free-based PSCs with A-cations, B-cations, and X-anions will be covered in the following sections.

A-site cation substitution The crystal structure, longevity and optoelectronic features of the perovskites are greatly influenced by the organic cation on the A-site of ABX_3 [81]. Regarding a Goldschmidt tolerance factor, A-site cation replacement must strictly be based on BX_6 octahedral sharing. The goal of A-site cation replacement is to achieve a more stable and dynamically suitable location for the perovskite film's energy levels [82]. Methylammonium (MA) and formamidinium (FA) are the two A-site organic cations in Pb-free OIHPs that have undergone the most comprehensive research. The sizes and functions of the A-cation may have a considerable impact on the perovskite lattice's dimensionality and durability. There is no doubt that MA^+ and FA^+ cations significantly affect the charge transfer and light absorption [83]. For example, combining MA^+ and FA^+ cations exhibit exceptional performance in the morphology of Pb-free perovskites and in the decrease of charge carrier recombination in a $(FA)_{0.75}(MA)_{0.25}$ SnI_3-based device, which led to a PCE of 8.12% [84].

It is widely documented that instability is mainly caused by the volatile cations like MA^+ and FA^+ in OIHPs. Therefore, using Cs^+ in place of MA^+ and FA^+ can produced a high level of environmental tolerance [85]. The stability of Cs^+ in Pb-free OIHPs was superior to that of the device utilizing $MAPbI_3$ for the same structural arrangement [86]. When employing MA^+ or Cs^+, Pb-free OIHPs are smaller than the identical material when using FA as the organic cation. It was found that lattice strain results due to the larger unit cells of $FASnI_3$ compared to the smaller unit cells of $MASnI_3$ and $CsSnI_3$ [87]. The most significant observation regarding Cs^+ is its inherent ability to improve stability in Pb-free PSCs. When exposed to ambient air, it exhibits a notable improvement in stability [88]. The volume of the perovskite rose as a result of the substitution of Cs^+ with MA^+ or FA^+, which also enhanced the bandgap [89]. In {en}$FASnI_3$-based PSCs, ethylenediammonium {en} as an organic cation boosted PCE to 7.14% and improved the device stability, as demonstrated in Fig. 6a–e [29]. In Pb-free PSCs, 2-phenylethyl alcohol was added as an organic cation, which improved the PCE to 6.98% [90]. These results demonstrate that the lattice polarizability of Pb-free OIHP is related to defect tolerance and does not necessitate the use of bigger organic cations like MA or FA [91]. It was also found that as the ionic radius of an organic cation increases, the octahedral deformation rises [92]. Likewise, the substitution of A-cation is responsible for expansion, contraction, or octahedral tilting, which might have a direct or indirect impact on the bandgap and optical characteristics of the Pb-free OIHPs. As the perovskites crystal lattices that are expanded by the large ionic radius at A-site with $Cs^+ < MA^+ < FA^+$ [81], therefore, it is crucial to pay close attention to Goldschmidt's tolerance factor in order to identify necessary organic cations, such as hydroxylammonium, hydrazinium, 3-pyrollinium, thiazolium, guanidinium, and potassium.

B-site cation substitution Due to its comparable electronic structure and close effective ionic radius to Pb, Sn^{2+} cation was the first divalent metal employed as an alternate candidate to substitute Pb^{2+} in order to produce Pb-free PSCs [93]. The first entirely Pb-free, $MASnI_3$-based PSCs, according to Noel et al. [26], achieved efficiencies of more than 6% under one-sun illumination. The neutrality between cations and anions in the perovskite structure, however, may be distorted by the oxidation process since Sn^{2+} displayed a tendency to oxidize into Sn^{4+} state. In this context, SnF_2 was added to $CsSnBr_3$ to slow down the fast oxidation of Sn when exposed to ambient air [94]. It was found that SnF_2 considerably increased the device's stability and PCE. Additional studies revealed that additional SnF_2 acted as a Sn^{4+} blocker in $FASnI_3$, resulted in a PCE of 4.8% in $FASnI_3$-based devices [95]. Mixing of MA and FA into SnI_2 produced high V_{oc} of 0.61 V, J_{sc} of 21.2 mA cm^{-2}, FF of 64.6%, and PCE of 8.12% [84]. Further experimental findings showed that creating a mixture of 2D/3D perovskite by combining PEA_2SnI_4 with $FASnI_3$ perovskite improved the morphology and orientation of the $FASnI_3$ grain, and the resulted device showed a high V_{oc} of 0.525 V, J_{sc} of 24.1 mA cm^{-2}, FF of 0.71, and PCE of 9.0%, as shown in Fig. 6f-j [96]. Using a Solar Cell Capacitance Simulator (SCAPS), Sajid et al. have examined a Pb-free perovskite homojunction-based HTM-free PSC and evaluated its performance [25]. To verify the simulation results, the researchers used a two-step procedure to fabricate Pb-free perovskite homojunction-based HTM-free PSCs. The simulation results showed that the V_{oc}, J_{sc}, FF, and PCE of $FASnI_3/CsSnI_3$ homojunction-based HTM-free PSCs were all enhanced from 0.66 to 0.78 V, 26.07 to 27.65 mA cm^{-2}, 76.37 to 79.74%, and 14.62 to 19.03%, respectively, when

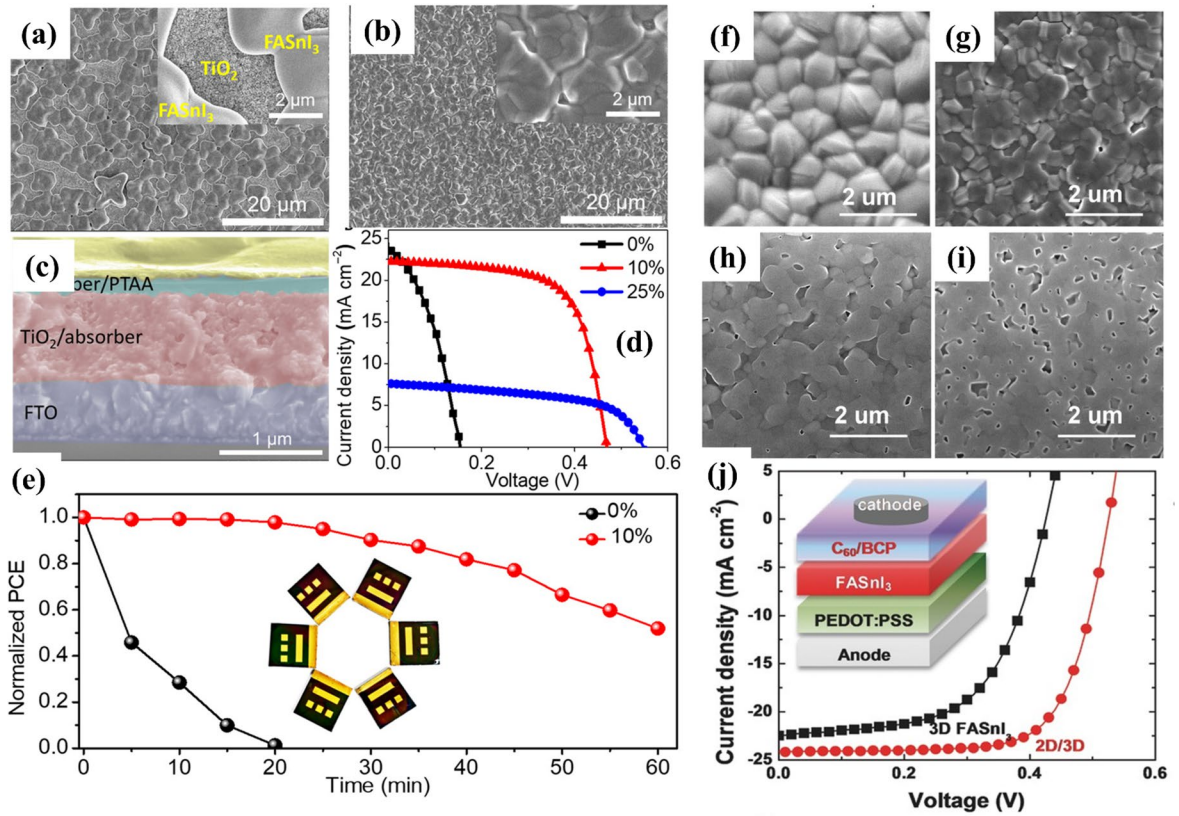

Fig. 6 **a**, **b** SEM images of the perovskite films without and with 10% of ethylenediammonium (insets: Top-view SEM images), **c** cross-sectional SEM image of the as-prepared device, **d** J-V curves of the PSCs using the perovskite layers with various amounts of ethylenediammonium addition, and **e** Aging test on the unsealed PSCs with and without 10% ethylenediammonium. **a**–**e** Reproduced with permission [29]. Copyright 2017, Science. **f**–**i** SEM images of $FASnI_3$ films with different 2D Sn-perovskite concentrations, and **j** J-V curves for the champion devices containing pure 3D and 2D/3D perovskite. **f**–**j** Reproduced with permission [96]. Copyright 2017, WILEY–VCH Verlag GmbH & Co. KGaA, Weinheim

compared to $FASnI_3$-based devices. An experimentally fabricated PSC employing homojunction of $FASnI_3$/$CsSnI_3$ showed a better PCE of 11.77% compared to $FASnI_3$-based device (PCE = 8.94%). Additionally, $FASnI_3$/$CsSnI_3$-based PSC preserved 89% of its initial PCE and was more stable over time than $FASnI_3$-based PSC. These findings offer encouraging guidance on developing PSCs that are both highly efficient and environmentally friendly.

Another viable option to replace Pb in PSCs is Ge. Due to the oxidation process, small ionic radius, broad bandgap (> 1.6 eV), poor solubility in polar solvents, and poor morphology, Ge-based OIHPs often exhibit low photovoltaic metrics [97]. The $MAGeI_3$ and $FAGeI_3$ demonstrated the best photovoltaic performance in Ge-based OIHPs when compared to guanidinium ($C[NH_2]GeI_3$), trimethyl-ammonium ($[CH_3]_3NHGeI_3$), acetamidinium ($CH_3C[NH_2]_2GeI_3$), and isopropylammonium ($[CH_3]_2C[H]NH_3GeI_3$ [19]. The Ge^{2+} cation can also be used to partially replace Sn^{2+} in order to form a thin oxidized layer on the surface that inhibits Sn^{2+} oxidation and enhance device performance. For instance, adding 5% Ge to $FA_{0.75}MA_{0.25}SnI_3$ perovskite [98] demonstrated that Ge is distributed on the material's surface and that it has the ability to successfully passivate perovskite traps and defects on the surface. As a result, 5% Ge doping produced a PCE of 4.48% (6.90% after 72 h of aging), which is a 35% improvement over the reference device (3.31%). In another study, the identical $FA_{0.75}MA_{0.25}Sn_{0.95}Ge_{0.05}I_3$ composition produced a champion PCE of 7.9% and a lower trap state density of 10^{15}–10^{17} cm^{-3} [74].

Because of its stability in ambient air, low toxicity, and straightforward fabrication procedure, bismuth (Bi) has also received considerable attention in attempts to replace Pb in OIHPs. Methylammonium bismuth iodide (MBI) in mesoporous PSCs was one of the first Bi-based OIHPs to be referred to, and it showed poor photocurrent, yielded very low PCE [56]. The indirect large bandgap may be the cause of this. The Cs^+ was substituted for MA^+ in the chemical structure of $CsBi_3I_{10}$, a photoactive perovskite, in order to increase photocurrent and decrease the bandgap in Bi-based perovskites [99]. The $CsBi_3I_{10}$-based device exhibited a 1.77 eV bandgap and displayed a PCE of 0.40%. The Bi-based perovskites are stable in ambient air, but nevertheless,

they possess lower PCEs due to wide bandgap. Because of its indirect bandgap (1.57 eV), which enables suitable light harvest, BiI_3 is a promising photoactive material in this context [100]. The mismatch in energy levels between BiI_3 and TiO_2 is the main obstacle to employing BiI_3 as an active material in PSCs. Both single BiI_3 and $A_3Bi_2I_9$ are unsuitable for efficient Pb-free PSCs in this aspect. As a result, using the chemical solution approach with active layers of BiI_3 and $A_3Bi_2I_9$ at room temperature produced better results [101]. The V_{oc} and PCE of the device increased from 0.44 V to 0.57 V and 0.045% to 0.076%, respectively. BiI_2 and MAI were both mixed in a typical solvents and spin-coated on a substrate as part of a one-step coating process, but this led to poor morphology and limited film coverage. This may be the obstacle to Bi-based perovskite's efficient solar energy conversion. Further research into highly efficient Bi-based PSCs has shown that a two-step process using sequential spin coatings of BiI_3 and MAI on a mesoporous TiO_2 increased PCE to 0.29% from the previously reported PCE [102].

The divalent Cu^{2+} cation is a viable substitute for Pb^{2+} in PSCs due to its abundance on earth, low toxicity, and excellent charge mobility. The Sn^{2+} and Ge^{2+} are less stable in ambient air than Cu^{2+} [97]. The 2D cupric bromide halide perovskite-based PSC displayed J_{sc} of 1.78 mA cm^{-2}, V_{oc} of 0.88 V, FF of 0.40%, and PCE of 0.63% [62]. Mixed halides have the potential to considerably enhance the stability of Cu-based perovskite. Small amounts of Cl have been found to improve crystallization and stability without impairing photovoltaic performance. For instance, the $(CH_3NH_3)_2CuCl_2Br_2$ and $(CH_3NH_3)_2CuCl_{0.5}Br_{3.5}$ have exhibited superior stability and the greatest PCEs of 0.017% compared to $(CH_3NH_3)_2CuCl_4$ and $(CH_3NH_3)_2CuClBr_3$ [103]. The synthesis of $(CH_3NH_3)_2CuX_4$ [$(CH_3NH_3)_2CuCl_4$, $(CH3NH_3)_2CuCl_2I_2$, and $(CH_3NH_3)_2CuCl_2Br_2$] was also reported [24], where Cl^- in the structure was discovered to be crucial for the stability of the produced compounds. The PSCs based on $(CH_3NH_3)_2CuCl_4$ yielded a PCE of 2.41% while $(CH_3NH_3)_2CuCl_2I_2$ and $(CH_3NH_3)_2CuCl_2Br_2$ produced PCEs of 1.75% and 0.99%, respectively. Nisha et al. [104] thoroughly investigated the synthesis of methylammonium bimetallic perovskites based on Sn and Cu of the general formula $CH_3NH_3Br.(SnBr_2)_{1x}(CuCl_2)_x$ as well as their structure, stability, and optoelectronic properties. These initial reports outline facile methods to develop stable and non-toxic OIHPs for photovoltaic applications.

Another appropriate element for Pb-free OIHPs is antimony (Sb). For instance, PCE of 4% in Sb-based PSC has been reported using bromoantimonate complexes containing both Sb (III) and Sb (V) [105]. Further research revealed that normal device (TiO_2/$(CH_3NH_3)_3Sb_2I_9$/spiro-OMeTAD) outperformed the inverted device (NiO/$(CH_3NH_3)_3Sb_2I_9$/PCMB), which is primarily due to the effective charge extraction, well-aligned energy levels, and high-quality thin-film fabrication [106]. The Cl inclusion in Sb-based OHIPs shown that it is possible to get stabilized 2D phase and restrict unwanted 0D pattern. For example, the $(CH_3NH_3)_3Sb_2Cl_xI_{9-x}$ was stabilized by Cl inclusion, which produced a PCE of 2.0% [107]. In $MASbSI_2$-perovskite, the use of sulfur and iodide as anions allowed the replacement of 2 + inorganic cations with 3 + and 4 + cations, and enabled Sb-based PSCs with a PCE of 3.08%, as can be seen in Fig. 7 [108]. Although the PCE was low, theoretical and experimental computations revealed that the bandgap of $(CH_3NH_3)_2AgSbI_6$ is around 1.93–2.0 eV, leading to highly stable PSCs [109]. The low PCE could be as a result of its poor morphology, which has numerous pinholes and poor light absorption. In this regard, the heterogeneous nucleation of the Sb-based perovskite was sped up while defect states were minimized using a mixed hydroiodic (HI)-chlorobenzene (CB) antisolvent. Final device consist of ITO/PEDOT:PSS/perylene/HI-CB-$(CH_3NH_3)_3Sb_2I_9$/$PC_{70}BM$/C_{60}/Al, displayed a PCE of 2.77% [110]. Other cations, including Ca^{2+}, Sr^{2+}, Mg^{2+}, and Zn^{2+}, can be utilized to substitute Pb in OIHPs in addition to Sn, Ge, Bi, and Sb, which is a potential area that should be further investigated [111].

X-site anion substitution Halides in OIHPs have the ability to alter the bandgaps and crystal structures while also enhancing stability. Iodine is the most often utilized halogen in Pb-free OIHPs. However, I^- has a relatively strong chemical reactivity, which makes vacancy defects simple to generate [112]. The Br^- has more electronegativity than I^-, therefore, it will lower the carrier density by preventing the creation of B-site cation vacancies and reducing cation oxidation [113]. In order to widen bandgaps and raise V_{oc}, Br^- can also alter crystal structures and upshift conduction energy levels. For instance, Br-doped $MASnI_3$ as light absorber demonstrated that bandgaps varied from 1.30 to 2.15 eV with a higher amount of Br^- [18], yielding in the best PSC with a PCE of 5.73% under 1-sun irradiation. Additionally, as I^- is gradually substituted by Br^-, the crystal structure changes from orthorhombic to greater symmetry, with optical bandgaps rising from 1.27 to 1.75 eV. In order to decrease carrier densities, Lee et al. inserted Br^- into the $FASnI_3$ lattice and produced bandgap shifts, reaching a PCE of 5.5% on adding 25 mol% of Br in $FASnI_3$ [114], as presented in Fig. 8. This Br-doped $FASnI_3$ PSC outperformed Pb-based device with the identical device design in terms of light stability under 1000 h of continuous 1-sun illumination [114]. Due to its small ionic radius and poor doping density, Cl^-, unlike I^- and Br^-, is rarely added to Pb-free OIHPs [115]. The MA-based ternary halide Sn-based perovskites ($MASnIBr_{2-x}Cl_x$) were fabricated by Tsai et al. [116] and it was found that the value of x cannot be greater than 1 without phase separation. A PCE of

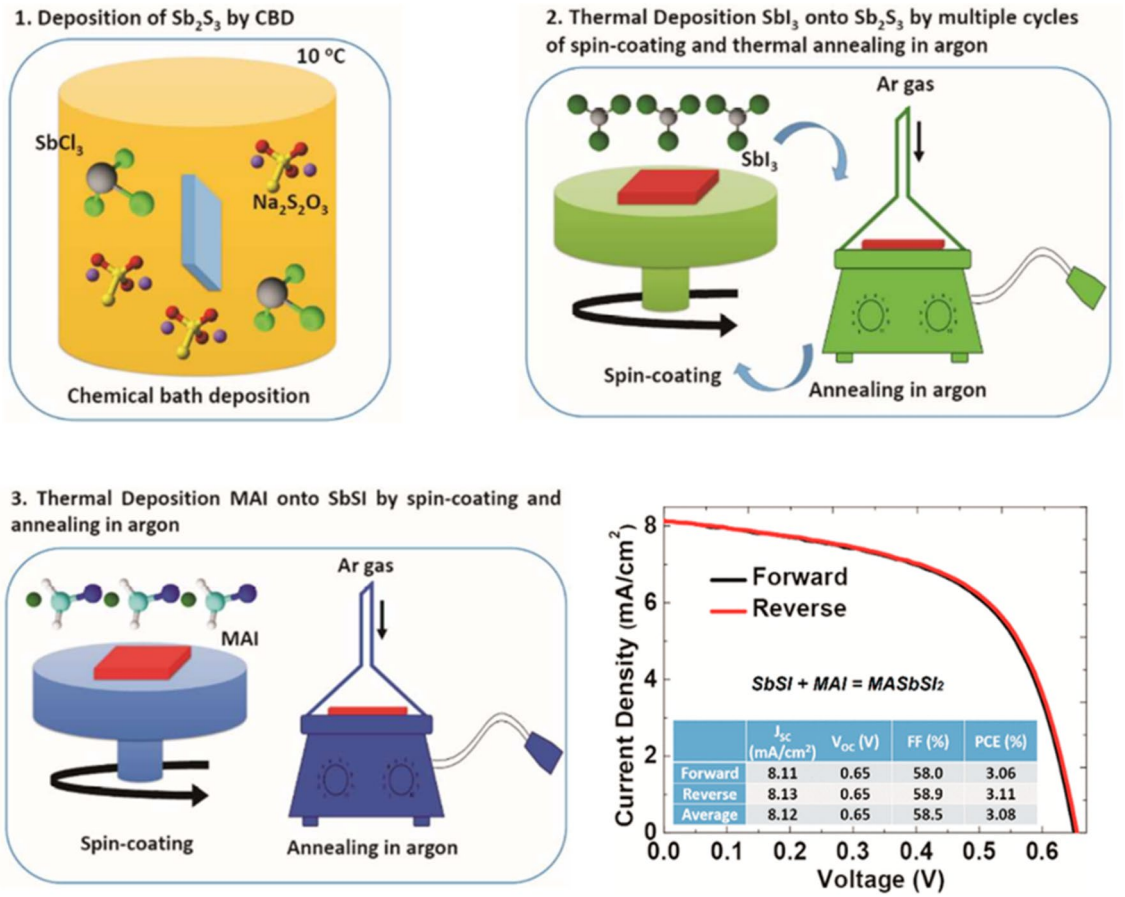

Fig. 7 Schematic illustration of preparing $MASbSI_2$ and J-V curves for the $MASbSI_2$-based PSCs (inset is the photovoltaic parameters). Reproduced with permission [108]. Copyright 2018, American Chemical Society

3.1% was achieved as a result of the charge recombination being impeded by a small quantity of Cl-doping. As widely recognized, compared to halide anions, pseudohalide anions such SCN^-, BF_4^-, PF_6^-, $HCOO^-$, and CH_3COO^- have certain special benefits that can control the nucleation and crystal growth while also enhancing the long-term stability of Pb-based perovskite films [117, 118]. Such a strategy is also promising for enhancing Pb-free OIHPs performance. For example, SCN^- was used by Rameez et al. to partially replace I^- to make $FASnI_{3-x}(SCN)_x$ perovskite. The SCN^- integration reduced nonradiative recombination and improved device stability in an environment with 65% relative humidity, leading to an increase in PCE (2.4%) as compared to $FASnI_3$-based device (0.9%) [119]. The performance of PSCs can be significantly enhanced by adding Br^- to the methylammonium germanium iodide perovskite, and the stability of the germanium perovskite can also be improved. According to Indira et al., PCEs up to 0.57% were produced in $MAGeI_{2.7}Br_{0.3}$-based solar cells by replacing 10% of the iodide with bromide [61]. A high-quality $(CH_3NH_3)_3Sb_2Cl_xI_{9-x}$ perovskite was produced as a result of Cl doping, which also considerably aided in producing layered phase structure and inhibited the undesirable 0D dimer phase [107]. By equimolar reaction of low-toxic $CuBr_2$ with hydrophobic $C_6H_4NH_2I$, Li et al. [63] synthesized $C_6H_4NH_2CuBr_2I$. Regardless the device's low PCE of 0.5%, the $C_6H_4NH_2CuBr_2I$ showed its benefits of low toxicity, high stability, and superb light absorption across the whole visible spectrum, which may address both the toxicity of Pb and the instability of perovskites [63].

To sum up, compositional engineering is a useful technique for enhancing the stability and efficacy of Pb-free OIHPs. But currently, relatively few research simultaneously varies the ions on various places; the majority of studies only alter the ions of the A-, B-, and X-site positions individually. As an instance, adding the phenylhydrazine cation ($PhNHNH^{3+}$), Cl^-, and Br^- to $FASnI_3$ produced a high PCE of 13.4% with outstanding light stability in PSC [120]. This is mostly related to the introduction of $PhNHNH^{3+}$ and halide anions, which control the nucleation and crystallization processes. The oxidation of $PhNHNH^{3+}$ further eliminated Sn^{4+} defects and prevented the aggregation of Br, while the

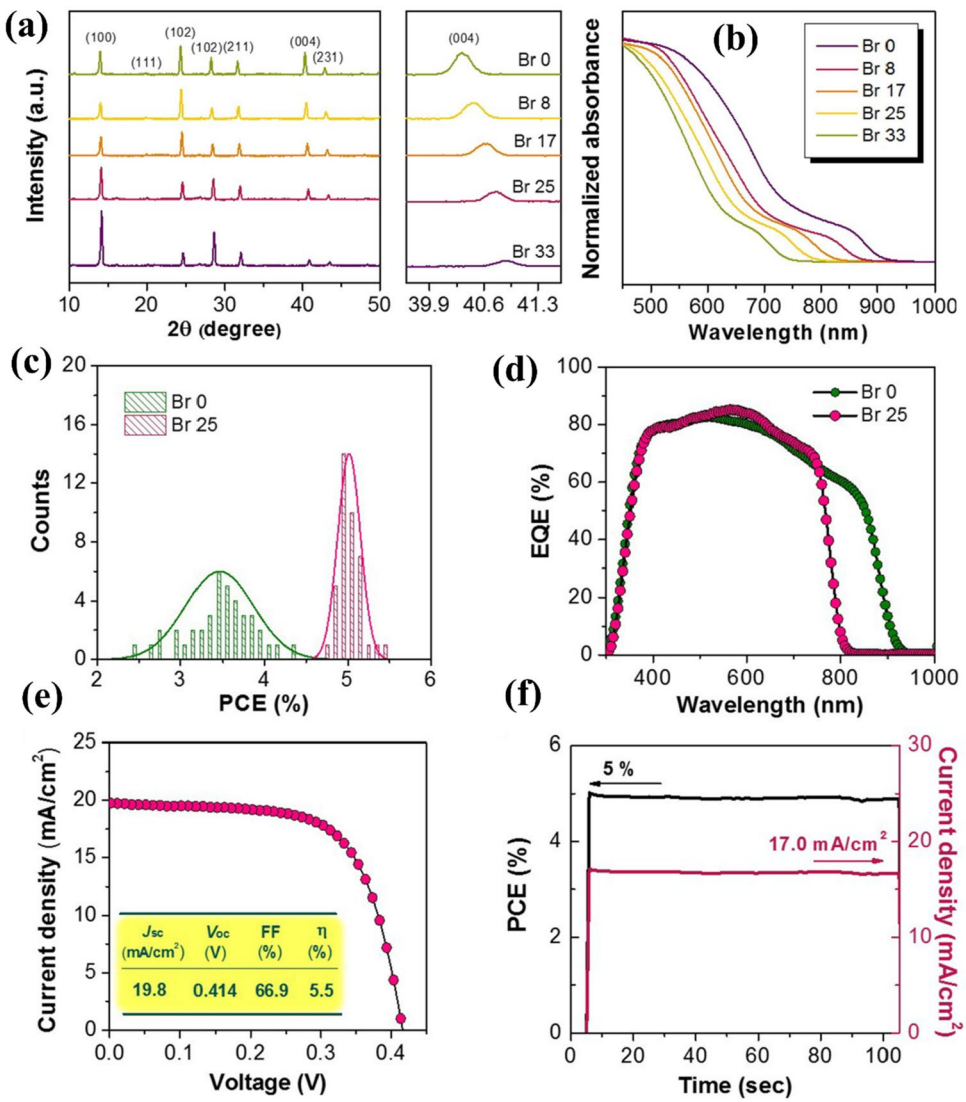

Fig. 8 **a** XRD patterns and **b** absorption spectra of $FASnI_3$ perovskite films with various Br content. **c** Histogram of PCE for 40 devices. **d** External quantum efficiency (EQE) of the optimized $FASnI_3$ and Br-doped $FASnI_3$ PSCs. **e** J-V curve of the device with the best performance and **f** stabilized PCE and photocurrent density of the best-performing device measured at a maximum power voltage of 0.293 V for 100 s. Reproduced with permission [114]. Copyright 2017, American Chemical Society

Br^- suppressed the I^- migration and reduced halide defects. This technique provided insight on how to further raise the stability and efficiency of the Pb-free PSCs.

Grain-boundaries passivation

Most Pb-free OIHP thin-films are polycrystalline and feature a high density of grain boundaries (GBs), which are directly responsible of accelerating ion migration/diffusion and oxygen/moist ingression. Additionally, the presence of numerous point defects at GBs, such as B-site vacancy defects, and undercoordinated cations/anions, etc. (Fig. 9a), would result in nonradiative recombination and the loss of photogenerated carriers, Voc, and PCE [121, 122]. The most significant point is that poorly oriented GBs have leaching channels that result in direct contact with charge transport layers below and above perovskite layers, resulting in small shunt resistances and short-circuit behaviors in PSCs. Thus, it is crucial to safeguard the GBs and passivate defects in order to produce highly efficient and stable PSCs. By forming hydrogen bonds between 5-ammonium valeric acid iodide (5-AVAI) and I^- of the $[SnI_6]_4$ octahedra, 5-AVAI additive into $FASnI_3$ films with SnF_2 efficiently passivated GBs of $FASnI_3$ films [123]. As a result, the Sn^{2+} oxidation was reduced and the crystallinity was improved, extending the carrier lifespan and raising the PCE from 3.4% to 7.0%. The oxidation stability of $FASnI_3$ was significantly improved by the potassium salts of hydroquinone sulfonic acid (KHQSA) and gallic acid (GA), which were combined with $SnCl_2$ to create $SnCl_2$-KHQSA and $SnCl_2$-GA complex capping layers at grain surfaces [124, 125]. Consequently, after being kept in ambient air with a 20% humidity level for 500 and 1000 h, respectively, the unsealed PSCs were able to maintain 80% of their initial PCEs. The performance of *N*,*N*-methylenebis(acrylamide) (MBAA) and thiosemicarbazide (TSC) additives in Pb-free perovskite was excellent

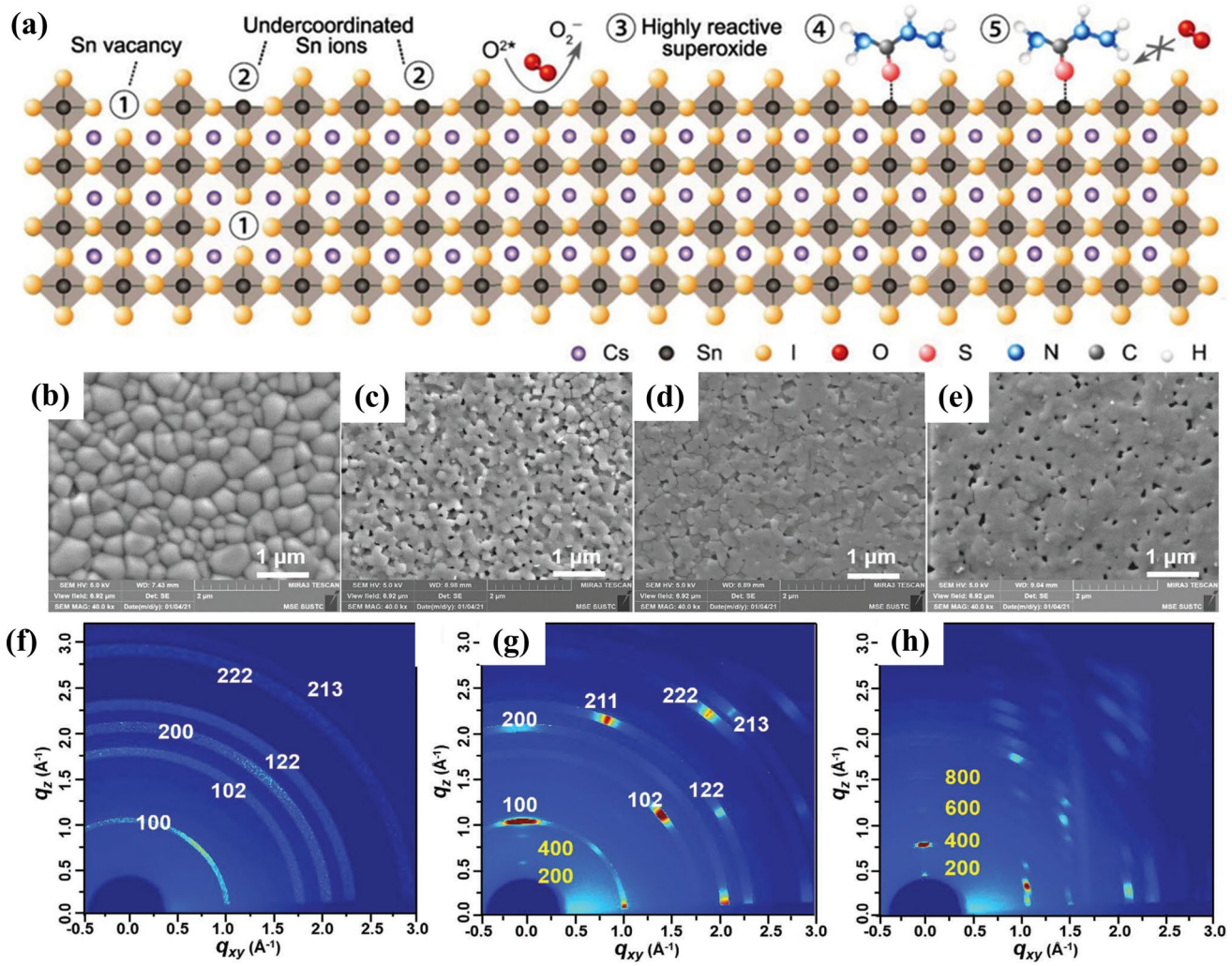

Fig. 9 **a** Schematic illustrating defects formed at the surface and in the interior of a $CsSnI_3$ perovskite and its corresponding passivation strategy, including (1) surface and interior Sn vacancy, (2) undercoordinated Sn ions, (3) proposed reaction pathway of superoxide production under photoexcitation, (4 and 5) Lewis acid–base interaction between thiosemicarbazide and $CsSnI_3$, and the resistance of oxidation. Reproduced with permission [121]. Copyright 2021, Wiley–VCH. **b–e** The SEM images of Sn-perovskite films with different FPEABr (0%, 5%, 10%, and 20%), **f–h** the GIWAXS images of 3D $FASnI_3$ film, 2D/3D mixture with 10% FPEABr, and FPEABr film, respectively. **b–h** Reproduced with permission [77]. Copyright 2021, Wiley–VCH

[121, 126], which was primarily attributed to the functional groups (-NH and -CO) in MBAA and S = C–N in TSC that have strong coordination with Sn^{2+} or charge defects at GBs, increasing electron density around defects and reducing defect densities.

In passivating GBs, the use of polymer has also produced encouraging results. For the fabrication of the $FASnI_3$ film, Zeng et al. employed α-methylstyrene (PAMS) as a polymer additive in the antisolvent diethyl ether [127]. The PAMS, which has a larger steric hindrance group than small-molecule additives, was primarily found on the surface of the $FASnI_3$ film because it did not readily penetrate the perovskite lattice. Pinholes on the surface of the $FASnI_3$ layer might be filled with PAMS, increasing hydrophobicity and lowering interfacial defects, which would then result in improved interfacial charge extraction. A self-encapsulation effect was demonstrated by poly (ethylene-co-vinyl acetate) (EVA) inclusion in antisolvent for perovskite crystallization during spin-coating [128], which could successfully stop moisture and oxygen from penetrating into the GBs of perovskite. Consequently, after aging for 48 h in air with a humidity of 60%, the PCE maintained 62.4% of the initial value. By replacing FAI with FPEABr in $FASnI_3$, Yu et al. [77] were able to successfully modify the microstructure of 2D/3D heterogeneous Sn-based OIHPs films. It was discovered in the optimal 2D/3D film that the 2D phase covered the 3D grains and was localized at the surfaces and GBs, as depicted in Fig. 9b-h. The addition of 2D phase can also

promote highly directed growth of 3D-$FASnI_3$. For inadequate 3D-$FASnI_3$ grains, the $FPEA^+$-based 2D Sn-perovskite capping layer could offer a reducing environment. The distinct microstructure successfully reduced defect density and efficiently suppressed the well-known oxidation from Sn^{2+} to Sn^{4+}, which resulted in a notable improvement in device PCE from 9.38% to 14.81%.

When compared to perovskite films formed on hydrophilic layers, it is known that substrates with hydrophobic surfaces/layers can increase grain size, produce fewer GBs, and result in improved film coverage. For instance, in order to reduce the amount of voids and improve the film quality, Priyadharsini et al. [110] added an interlayer that served as a good hydrophobic scaffold for the formation of large-grain $(CH_3NH_3)_3Sb_2I_9$ crystals, and achieved a PCE of 2.77%. The fabrication techniques are crucial for producing perovskite layers of the highest quality. For instance, high-quality $MASbSI_2$ was made by sequentially reacting antimony trisulfide (Sb_2S_3), which was deposited onto a mesoporous TiO_2 using the chemical bath deposition method, and thermal deposition of antimony triiodide (SbI_3) and methylammonium iodide (MAI). Under standard illumination conditions of 100 mW/cm^2, the PSC made with $MASbSI_2$ displayed PCE of 3.08% [108]. Similarly, by thermally evaporating BiI_3, spin-coating MAI solution to create a BiI_3/MAI stacking layer first, and then in situ forming $MA_3Bi_2I_9$ upon post-annealing by a molecule interdiffusion process, Ran et al. [129] constructed uniform and pinhole-free $MA_3Bi_2I_9$ thin-films. The distinguishing MBI and its high-quality photoactive thin-films were more significant when deposited using a two-step, solvent-contact-free high-low vacuum method [130]. This method produced MBI films that were just as completely compact as the $MAPbI_3$ films, greatly improved the final performance of MBI solar cells. According to statistics in Table 1, the Sn-based PSCs often have higher efficiency than other Pb-free PSCs. The Sn-based PSCs have improved and have closed the efficiency gap, albeit Pb-based devices still marginally outperform them. Because Sn is more abundant and less expensive than Pb, it can be produced more affordably than Pb-based PSCs. Moreover, Sn-based OIHPs offer the advantage of tunable bandgaps, which can be adjusted for specific applications. This flexibility allows for the optimization of the perovskite material to capture light in different parts of the solar spectrum, improving overall efficiency.

Conclusions and future prospects

The review suggests that the Sn-based perovskites appear to hold promises for obtaining excellent performance in the near future. However, even with sealing, the Sn-based perovskites are much less stable than the Pb-based ones. The stability problems can be further addressed by combining the technological advances of the Sn and Pb-based perovskites. However, until the stability issue is resolved, we are unable to determine whether they are viable choices. Recently, PCEs of 14% are obtained for Sn-based PSCs [162]. The V_{oc} of about 0.8 to more than 1.0 V should be possible after the Sn^{4+} oxidation issue is fully resolved and photocarrier recombination rates are decreased to the levels of the Pb-based OIHPs. Then, PCE will have the option of going above 15%, greatly enhancing their chances of becoming a competitive Pb-free candidate. Ge-based perovskites are not the best as Sn-based perovskites. The mixed Ge/Sn-based perovskites, however, seem attractive if further research can achieve the efficiency levels above 10% [74]. Future studies will require more research to fully grasp the enhancement of stability. The extraordinarily high price of Ge is one potential issue with Ge-based PSCs. Bismuth, Bi^{3+}, is an isoelectronic to Pb^{2+} with a nearly identical effective ionic radius and the same lone pair. The Bi-based OIHPs gained interest because of their non-toxicity, environmental stability, and straightforward solution processing. The Bi-based OIHPs, however, had a relatively poor PCE because to a too-large bandgap. Cu has the proper oxidation state to take the place of Pb, but because of its smaller ionic radius, the corner sharing system of the halide octahedral structure can become compromised. The Sn^{2+} and Ge^{2+} are less stable than Cu^{2+}. The $(CH_3NH_3)_2CuCl_4$-based device showed a PCE of 2.41% [24]. Due to its excellent optoelectronic characteristics and tendency for formation in many structural dimensions, Sb is an additional option to Pb. The Sb-based OIHPs have a PCE of roughly 2.77%. In order to further enhance the PCEs of Sb-based PSCs, a better thin-film morphology free of pinholes must be attained.

The Pb-free OIHPs currently offer an undesirable options, for example, high efficiency but poor stability (Sn^{2+}-based) or favorable stability but poor performance (Sn/Bi/Cu/Sb-based, etc.). Can we find a suitable Pb-free OIHP that combines good optoelectronic and stable properties? We hope that additional investigations will pay attention to this problem. Even though the total Pb weight of a 500 nm thick perovskite film in solar cells may be minimal, the development of Pb-free PSCs is unquestionably a worthwhile goal, and device innovation will offer a convincing viable solution, including ways to recycle Pb-based OIHPs. Potential candidates should not be restricted to the OIHP families; instead, new materials including chalcogenide perovskites and non-perovskites with novel structures merit further study. Undoubtedly, the most promising candidates should be able to maintain initial high PCEs for 1000 h under 85 °C and 85% relative humidity, as well as be low-cost, scalable, and most importantly stable enough to meet the industrial requirements. The Pb-free PSCs are still in the early stages of development and are interesting; the future is promising,

Table 1 Summary of the PSC performance utilizing Pb-free OHIPs

Composition	PCE (%)	J_{sc} (mA cm^{-2})	V_{oc} (V)	FF (%)	Refs
$MASnI_3$	6.4	16.8	0.88	42.0	[26]
$MASnI_3$	3.15	21.4	0.32	46.0	[79]
$MASnIBr_2$	5.73	12.3	0.82	57.0	[18]
$FASnI_3$ (SnF_2, pyrazine)	4.8	23.7	0.32	63.0	[95]
$FASnI_3$ (SnF_2)	6.22	22.07	0.46	60.67	[131]
$FASnI_3$ (PPA)	9.61	23.34	0.56	73.5	[132]
$FASnI_3$ (SnF_2, CDTA)	10.1	21.22	0.63	74.7	[133]
$FA_{0.75}MA_{0.25}SnI_3$	8.12	21.2	0.61	62.7	[84]
{en}$FASnI_3$ (SnF_2)	7.23	22.54	0.46	69.74	[134]
{en}$FASnI_3$ (SnF_2)	7.59	22.41	0.49	68.21	[135]
$PEA_{0.08}FA_{0.92}SnI_3$ (SnF_2)	9.0	24.1	0.53	71.0	[96]
$FASnI_3$ (SnF_2, TMA)	7.09	22.45	0.47	67.8	[136]
$FASnI_3$ (SnF_2, LFA)	10.37	22.25	0.62	74.2	[137]
$FASnI_3$ (SnF_2, FOEI)	10.81	21.59	0.67	75.0	[138]
$FASnI_3$ (PHCl)	11.4	23.5	0.76	64.0	[139]
$FASnI_3$ (SnF_2, PAI)	11.78	22.37	0.73	72.0	[140]
$FASnI_3$ (SnF_2, PAI)	12.11	22.48	0.77	70.0	[141]
$FASnI_3$ (5-AVAI)	7.0	18.89	0.59	62.3	[123]
$FASnI_3$ ($SnCl_2$)	10.47	22.71	0.63	73.2	[142]
$PEA_{0.1}FA_{0.9}SnI_3$ (SnF_2,FASCN)	8.17	22.5	0.53	68.3	[143]
$PEA_{0.15}FA_{0.85}SnI_3$ (SnF_2,NH_4SCN)	9.41	22.0	0.61	70.1	[144]
$GA_{0.2}FA_{0.8}SnI_3$ (SnF_2,$EDAI_2$)	9.6	21.2	0.61	72.9	[145]
$PEA_{0.08}FA_{0.92}SnI_3$ (SnF_2, EAI)	8.4	23.75	0.51	70.0	[146]
$(BA_{0.5}PEA_{0.5})_2FA_3Sn_4I_{13}$ (SnF_2,GAI)	8.82	21.82	0.60	66.73	[147]
$(BEA)FA_2Sn_3I_{10}$	6.43	18.85	0.62	55.0	[148]
$PEA_{0.15}FA_{0.85}SnI_3$ (SnF_2, NH_4SCN)	12.4	17.4	0.94	75.0	[138]
$(FA_{0.9}EA_{0.1})_{0.98}EDA_{0.01}SnI_3$ (SnF_2, GeI_2)	13.24	20.32	0.84	78.0	[149]
$FA_{0.75}MA_{0.25}SnI_3$ (TM-DHP, EDA)	11.5	22.0	0.76	69.0	[150]
$GA_{0.2}FA_{0.8}SnI_3$-1% $EDAI_2$ (AN)	10.4	21.1	0.65	76.3	[151]
$FA_{0.9}AcA_{0.1}SnI_3$ (SnF_2)	8.11	21.05	0.56	69.3	[152]
$(PEA)_{0.2}(FA)_{0.8}SnI_3$ (SnF_2)	10.0	22.9	0.60	73.0	[153]
$PEA_{0.15}FA_{0.85}SnI_3$ (SnF_2, NH_4SCN)	14.6	20.6	0.91	77.1	[154]
$FASnI_3$ (FPEABr, SnF_2)	14.81	24.91	0.84	71.0	[77]
$FAPEASnBrI_2$ (SnF_2, NH_4SCN, 2-Guanidinoacetic acid)	13.70	19.66	0.93	74.9	[155]
$FAPEASnBrI_2$ (SnF_2, NH_4SCN, $InBr_3$)	14.02	18.89	1.013	73.22	[156]
$(CH_3NH_3)_3Bi_2I_9$	0.11	0.49	0.72	31.8	[62]
$(CH_3NH_3)_3Bi_2I_9$	0.22	0.38	0.68	88.0	[129]
$(CH_3NH_3)_3Bi_2I_9$	0.12	0.52	0.68	33.0	[157]
$(CH_3NH_3)_3Bi_2I_9$	0.19	1.157	0.35	46.4	[99]
$(CH_3NH_3)_3Bi_2I_9$	0.71	1.22	0.85	73.0	[106]
$(CH_3NH_3)_3Bi_2I_9$	0.39	1.39	0.83	37.0	[51]
$(CH_3NH_3)_3Bi_2I_9$	1.64	3.0	0.83	79.0	[72]
$(CH_3NH_3)_3Bi_2I_9$	3.17	1.01	4.02	78.0	[56]
$(CH_3NH_3)_3Bi_2I_9Cl_x$	0.03	0.18	0.04	38.0	[157]
$(CH_3NH_3)_3Bi_2I_9$	0.39	1.39	0.83	34.0	[129]
$(CH_3NH_3)_3Bi_2I_9$	1.62	2.70	0.76	69.0	[158]
$(CH_3NH_3)_3Bi_2I_{9-2x}S_x$	0.152	0.58	0.54	47.6	[159]
$CH_3NH_3PbBr_3$ (1% Bi & 1% Sb)	11.6	12.12	1.32	73.0	[160]
$CH_3NH_3GeI_3$	0.20	4.0	0.15	30.0	[52]
$CH_3NH_3GeI_{2.7}Br_{0.3}$	0.68	3.11	0.46	48.0	[61]

Table 1 (continued)

Composition	PCE (%)	J_{sc} (mA cm^{-2})	V_{oc} (V)	FF (%)	Refs
$FA_{0.75}MA_{0.25}Sn_{1-x}Ge_xI_3$	7.9	25.58	0.45	69.0	[74]
$FA_{0.92}PEA_{0.08}Sn_xGe_{1-x}I_3$	7.45	21.92	0.46	73.0	[75]
$(CH_3NH_3)_3Sb_2I_9$	2.25	5.09	0.62	59.89	[110]
$(CH_3NH_3)_3Sb_2I_9$	2.77	6.64	0.70	59.60	[76]
$(CH_3NH_3)_3Sb_2I_9$	0.49	1.0	0.896	55.0	[58]
$CH_3NH_3SbSI_2$	3.08	8.12	0.65	58.5	[108]
$(CH_3NH_3)_3Sb_2Cl_xI_{9-x}$	2.19	5.04	0.69	63.0	[107]
$(CH_3NH_3)_3Sb_2I_9$	2.04	5.41	0.62	60.82	[59]
$(CH_3NH_3)_3(Sb_{1-x}Sn_x)_2I_9$	2.70	8.32	0.56	58.0	[161]
$(NH_4)_3Sb_2I_xBr_{9-x}$	0.51	1.15	1.03	42.9	[76]
$(CH_3NH_3)_2CuCl_2Br_2$	0.017	0.216	0.256	32.0	[103]
$CH_3(CH_2)_3NH_3)_2$–$CuBr_4$	0.63	1.78	0.88	40.0	[62]
$C_6H_4NH_2CuBr_2I$	0.46	6.20	0.20	46.0	[63]
$(C_6H_5CH_2NH_3)_2CuBr_4$	0.20	0.73	0.68	41.0	[20]
$(CH_3NH_3)_2CuCl_4$	2.41	8.12	0.560	52.0	[64]
$(CH_3NH_3)_2CuCl_2I_2$	1.75	6.78	0.545	47.0	[64]
$(CH_3NH_3)_2CuCl_2Br_2$	0.99	3.35	0.581	50.0	[64]

particularly as more research and investment efforts are made.

Acknowledgements This work was financially supported by the UAEU-Strategic research program under Grant no.12R128.

Author contributions Conceptualization, SS, IMO, and SA; Supervision and validation, IMO, SA, and IBS; Formal analysis, NT.; YAH and IMO; Investigation, SS; Methodology, SS; Writing, SS; Review & editing, IMO SS and NT The final version of the manuscript has been approved by all contributors.

Data availability Not applicable because it is review paper.

Declaration

Conflict of interest The authors do not have any conflicts of interest to disclose.

References

1. Sun, J., Wu, J., Tong, X., Lin, F., Wang, Y., Wang, Z.M.: Organic/inorganic metal halide perovskite optoelectronic devices beyond solar cells. Adv. Sci. **5**, 1700780 (2018). https://doi.org/10.1002/advs.201700780
2. Green, M.A., Dunlop, E.D., Siefer, G., Yoshita, M., Kopidakis, N., Bothe, K., Hao, X.: Solar cell efficiency tables (Version 61). Prog. Photovoltaics Res. Appl. **31**, 3–16 (2023). https://doi.org/10.1002/pip.3646
3. Wei, D., Ma, F., Wang, R., Dou, S., Cui, P., Huang, H., Ji, J., Jia, E., Jia, X., Sajid, S., Elseman, A.M., Chu, L., Li, Y., Jiang, B., Qiao, J., Yuan, Y., Li, M.: Ion-Migration inhibition by the cation–π interaction in perovskite materials for efficient and stable perovskite solar cells. Adv. Mater. **30**, 1707583 (2018). https://doi.org/10.1002/adma.201707583
4. Wei, D., Huang, H., Cui, P., Ji, J., Dou, S., Jia, E., Sajid, S., Cui, M., Chu, L., Li, Y., Jiang, B., Li, M.: Moisture-tolerant supermolecule for the stability enhancement of organic–inorganic perovskite solar cells in ambient air. Nanoscale **11**, 1228–1235 (2019). https://doi.org/10.1039/C8NR07638C
5. Elseman, A.M., Sharmoukh, W., Sajid, S., Cui, P., Ji, J., Dou, S., Wei, D., Huang, H., Xi, W., Chu, L., Li, Y., Jiang, B., Li, M.: Superior stability and efficiency over 20% perovskite solar cells achieved by a novel molecularly engineered Rutin–AgNPs/Thiophene copolymer. Adv. Sci. **5**, 1800568 (2018). https://doi.org/10.1002/advs.201800568
6. M. Yang, T. Tian, Y. Fang, W.-G. Li, G. Liu, W. Feng, M. Xu, W.-Q. Wu, Reducing lead toxicity of perovskite solar cells with a built-in supramolecular complex, Nat. Sustain. (2023) 1–10.
7. W. Zhang, H. Liu, F. Yan, B. Dong, H. Wang, Recent Progress of Low-Toxicity Poor-Lead All-Inorganic Perovskite Solar Cells, Small Methods. (2023) 2300421.
8. Hailegnaw, B., Kirmayer, S., Edri, E., Hodes, G., Cahen, D.: Rain on methylammonium lead iodide based perovskites: possible environmental effects of perovskite solar cells. J. Phys. Chem. Lett. **6**, 1543–1547 (2015). https://doi.org/10.1021/acs.jpclett.5b00504
9. Lyu, M., Yun, J.-H., Chen, P., Hao, M., Wang, L.: Addressing toxicity of lead: progress and applications of low-toxic metal halide perovskites and their derivatives. Adv. Energy Mater. **7**, 1602512 (2017). https://doi.org/10.1002/aenm.201602512

10. Wang, R., Wang, J., Tan, S., Duan, Y., Wang, Z.-K., Yang, Y.: Opportunities and challenges of lead-free perovskite optoelectronic devices. Trends Chem. **1**, 368–379 (2019). https://doi.org/10.1016/j.trechm.2019.04.004
11. Giustino, F., Snaith, H.J.: Toward lead-free perovskite solar cells. ACS Energy Lett. **1**, 1233–1240 (2016). https://doi.org/10.1021/acsenergylett.6b00499
12. Ren, M., Qian, X., Chen, Y., Wang, T., Zhao, Y.: Potential lead toxicity and leakage issues on lead halide perovskite photovoltaics. J. Hazard. Mater. **426**, 127848 (2022). https://doi.org/10.1016/j.jhazmat.2021.127848
13. Su, P., Liu, Y., Zhang, J., Chen, C., Yang, B., Zhang, C., Zhao, X.: Pb-based perovskite solar cells and the underlying pollution behind clean energy: dynamic leaching of toxic substances from discarded perovskite solar cells. J. Phys. Chem. Lett. **11**, 2812–2817 (2020). https://doi.org/10.1021/acs.jpclett.0c00503
14. Li, Z., Wu, X., Wu, S., Gao, D., Dong, H., Huang, F., Hu, X., Jen, A.K.-Y., Zhu, Z.: An effective and economical encapsulation method for trapping lead leakage in rigid and flexible perovskite photovoltaics. Nano Energy **93**, 106853 (2022)
15. Li, J., Cao, H.-L., Jiao, W.-B., Wang, Q., Wei, M., Cantone, I., Lü, J., Abate, A.: Biological impact of lead from halide perovskites reveals the risk of introducing a safe threshold. Nat. Commun. **11**, 310 (2020)
16. Jiang, Y., Qiu, L., Juarez-Perez, E.J., Ono, L.K., Hu, Z., Liu, Z., Wu, Z., Meng, L., Wang, Q., Qi, Y.: Reduction of lead leakage from damaged lead halide perovskite solar modules using self-healing polymer-based encapsulation. Nat. Energy **4**, 585–593 (2019)
17. Li, X., Zhang, F., He, H., Berry, J.J., Zhu, K., Xu, T.: On-device lead sequestration for perovskite solar cells. Nature **578**, 555–558 (2020)
18. Hao, F., Stoumpos, C.C., Cao, D.H., Chang, R.P.H., Kanatzidis, M.G.: Lead-free solid-state organic–inorganic halide perovskite solar cells. Nat. Photonics **8**, 489–494 (2014)
19. Stoumpos, C.C., Frazer, L., Clark, D.J., Kim, Y.S., Rhim, S.H., Freeman, A.J., Ketterson, J.B., Jang, J.I., Kanatzidis, M.G.: Hybrid germanium iodide perovskite semiconductors: active lone pairs, structural distortions, direct and indirect energy gaps, and strong nonlinear optical properties. J. Am. Chem. Soc. **137**, 6804–6819 (2015)
20. Li, X., Li, B., Chang, J., Ding, B., Zheng, S., Wu, Y., Yang, J., Yang, G., Zhong, X., Wang, J.: (C6H5CH2NH3) 2CuBr 4: a lead-free, highly stable two-dimensional perovskite for solar cell applications. ACS Appl. Energy Mater. **1**, 2709–2716 (2018)
21. Wang, M., Zeng, P., Bai, S., Gu, J., Li, F., Yang, Z., Liu, M.: High-quality sequential-vapor-deposited Cs2AgBiBr 6 thin films for lead-free perovskite solar cells. Sol. Rrl. **2**, 1800217 (2018)
22. Igbari, F., Wang, R., Wang, Z.-K., Ma, X.-J., Wang, Q., Wang, K.-L., Zhang, Y., Liao, L.-S., Yang, Y.: Composition stoichiometry of Cs2AgBiBr 6 films for highly efficient lead-free perovskite solar cells. Nano Lett. **19**, 2066–2073 (2019)
23. Slavney, A.H., Hu, T., Lindenberg, A.M., Karunadasa, H.I.: A bismuth-halide double perovskite with long carrier recombination lifetime for photovoltaic applications. J. Am. Chem. Soc. **138**, 2138–2141 (2016)
24. Elseman, A.M., Shalan, A.E., Sajid, S., Rashad, M.M., Hassan, A.M., Li, M.: Copper-substituted lead perovskite materials constructed with different halides for working (CH3NH3)2CuX4-based perovskite solar cells from experimental and theoretical view. ACS Appl. Mater. Interfaces **10**, 11699–11707 (2018). https://doi.org/10.1021/acsami.8b00495
25. S. Sajid, S. Alzahmi, I.B. Salem, J. Park, I.M. Obaidat, lead-free perovskite homojunction-based HTM-free perovskite solar cells: theoretical and experimental viewpoints, Nanomaterials. 13 (2023). https://doi.org/10.3390/nano13060983.
26. Noel, N.K., Stranks, S.D., Abate, A., Wehrenfennig, C., Guarnera, S., Haghighirad, A.-A., Sadhanala, A., Eperon, G.E., Pathak, S.K., Johnston, M.B.: Lead-free organic–inorganic tin halide perovskites for photovoltaic applications. Energy Environ. Sci. **7**, 3061–3068 (2014)
27. Saidaminov, M.I., Spanopoulos, I., Abed, J., Ke, W., Wicks, J., Kanatzidis, M.G., Sargent, E.H.: Conventional solvent oxidizes Sn (II) in perovskite inks. ACS Energy Lett. **5**, 1153–1155 (2020)
28. Nasti, G., Abate, A.: Tin halide perovskite (ASnX3) solar cells: a comprehensive guide toward the highest power conversion efficiency. Adv. Energy Mater. **10**, 1902467 (2020)
29. Ke, W., Stoumpos, C.C., Zhu, M., Mao, L., Spanopoulos, I., Liu, J., Kontsevoi, O.Y., Chen, M., Sarma, D., Zhang, Y.: Enhanced photovoltaic performance and stability with a new type of hollow 3D perovskite en FASnI3. Sci. Adv. **3**, e1701293 (2017)
30. Borriello, I., Cantele, G., Ninno, D.: Ab initio investigation of hybrid organic-inorganic perovskites based on tin halides. Phys. Rev. B **77**, 235214 (2008)
31. Umari, P., Mosconi, E., De Angelis, F.: Relativistic GW calculations on CH3NH3PbI3 and CH3NH3SnI3 perovskites for solar cell applications. Sci. Rep. **4**, 4467 (2014)
32. Liu, Y., Yang, Z., Liu, S.: Recent progress in single-crystalline perovskite research including crystal preparation, property evaluation, and applications. Adv. Sci. **5**, 1700471 (2018)
33. Prasanna, R., Gold-Parker, A., Leijtens, T., Conings, B., Babayigit, A., Boyen, H.-G., Toney, M.F., McGehee, M.D.: Band gap tuning via lattice contraction and octahedral tilting in perovskite materials for photovoltaics. J. Am. Chem. Soc. **139**, 11117–11124 (2017)
34. Goyal, A., McKechnie, S., Pashov, D., Tumas, W., Van Schilfgaarde, M., Stevanovic, V.: Origin of pronounced nonlinear band gap behavior in lead–tin hybrid perovskite alloys. Chem. Mater. **30**, 3920–3928 (2018)
35. A.R. bin M. Yusoff, M.K. Nazeeruddin,: Organohalide lead perovskites for photovoltaic applications. J. Phys. Chem. Lett. **7**, 851–866 (2016)
36. Y. Liu, S. Yuan, H. Zheng, M. Wu, S. Zhang, J. Lan, W. Li, J. Fan, Structurally Dimensional Engineering in Perovskite Photovoltaics, Adv. Energy Mater. (2023) 2300188.
37. Yuan, S., Liu, Y., Lan, J., Yang, W., Xiong, H., Li, W., Fan, J.: Accurate dimension prediction for low-dimensional organic-inorganic halide perovskites via a self-established machine learning strategy. J. Phys. Chem. Lett. **14**, 7323–7330 (2023)
38. Xiao, Z., Meng, W., Wang, J., Mitzi, D.B., Yan, Y.: Searching for promising new perovskite-based photovoltaic absorbers: the importance of electronic dimensionality. Mater. Horizons. **4**, 206–216 (2017)
39. J.-P. Correa-Baena, M. Saliba, T. Buonassisi, M. Grätzel, A. Abate, W. Tress, A. Hagfeldt, Promises and challenges of perovskite solar cells, Science (80-.). 358 (2017) 739–744.
40. Wang, B., Xiao, X., Chen, T.: Perovskite photovoltaics: a high-efficiency newcomer to the solar cell family. Nanoscale **6**, 12287–12297 (2014)
41. Rühle, S.: Tabulated values of the Shockley-Queisser limit for single junction solar cells. Sol. Energy **130**, 139–147 (2016)
42. Ogomi, Y., Morita, A., Tsukamoto, S., Saitho, T., Fujikawa, N., Shen, Q., Toyoda, T., Yoshino, K., Pandey, S.S., Ma, T.: CH3NH3Sn x Pb (1–x) I3 Perovskite solar cells covering up to 1060 nm. J. Phys. Chem. Lett. **5**, 1004–1011 (2014)
43. Cao, D.H., Stoumpos, C.C., Yokoyama, T., Logsdon, J.L., Song, T.-B., Farha, O.K., Wasielewski, M.R., Hupp, J.T., Kanatzidis, M.G.: Thin films and solar cells based on semiconducting two-dimensional ruddlesden–popper (CH3 (CH2) 3NH3) 2 (CH3NH3) n− 1Sn n I3 n+ 1 perovskites. ACS Energy Lett. **2**, 982–990 (2017)

44. Grancini, G., Nazeeruddin, M.K.: Dimensional tailoring of hybrid perovskites for photovoltaics. Nat. Rev. Mater. **4**, 4–22 (2019)
45. Abbas, M.S., Hussain, S., Zhang, J., Wang, B., Yang, C., Wang, Z., Wei, Z., Ahmad, R.: Orientationally engineered 2D/3D perovskite for high efficiency solar cells, Sustain. Energy Fuels **4**, 324–330 (2020)
46. Schmickler, W., Santos, E., Bronshtein, M., Nazmutdinov, R.: Adiabatic electron-transfer reactions on semiconducting electrodes. ChemPhysChem **18**, 111–116 (2017)
47. Gong, J., Guo, P., Benjamin, S.E., Van Patten, P.G., Schaller, R.D., Xu, T.: Cation engineering on lead iodide perovskites for stable and high-performance photovoltaic applications. J. Energy Chem. **27**, 1017–1039 (2018)
48. Herz, L.M.: Charge-carrier mobilities in metal halide perovskites: fundamental mechanisms and limits. ACS Energy Lett. **2**, 1539–1548 (2017)
49. Ma, L., Hao, F., Stoumpos, C.C., Phelan, B.T., Wasielewski, M.R., Kanatzidis, M.G.: Carrier diffusion lengths of over 500 nm in lead-free perovskite CH3NH3SnI3 films. J. Am. Chem. Soc. **138**, 14750–14755 (2016)
50. Song, T.-B., Yokoyama, T., Stoumpos, C.C., Logsdon, J., Cao, D.H., Wasielewski, M.R., Aramaki, S., Kanatzidis, M.G.: Importance of reducing vapor atmosphere in the fabrication of tin-based perovskite solar cells. J. Am. Chem. Soc. **139**, 836–842 (2017). https://doi.org/10.1021/jacs.6b10734
51. R.L.Z. Hoye, R.E. Brandt, A. Osherov, V. Stevanović, S.D. Stranks, M.W.B. Wilson, H. Kim, A.J. Akey, J.D. Perkins, R.C. Kurchin, J.R. Poindexter, E.N. Wang, M.G. Bawendi, V. Bulović, T. Buonassisi, Methylammonium Bismuth Iodide as a Lead-Free, Stable Hybrid Organic–Inorganic Solar Absorber, Chem.—A Eur. J. 22 (2016) 2605–2610. https://doi.org/10.1002/chem.201505055.
52. Krishnamoorthy, T., Ding, H., Yan, C., Leong, W.L., Baikie, T., Zhang, Z., Sherburne, M., Li, S., Asta, M., Mathews, N., Mhaisalkar, S.G.: Lead-free germanium iodide perovskite materials for photovoltaic applications. J. Mater. Chem. A. **3**, 23829–23832 (2015). https://doi.org/10.1039/C5TA05741H
53. Kawai, T., Ishii, A., Kitamura, T., Shimanuki, S., Iwata, M., Ishibashi, Y.: Optical absorption in band-edge region of (CH 3 NH 3) 3 B i 2 I 9 single crystals. J. Phys. Soc. Japan. **65**, 1464–1468 (1996)
54. Jakubas, R., Zaleski, J., Sobczyk, L.: Phase transitions in (CH3NH3) 3Bi2I9 (MAIB). Ferroelectrics **108**, 109–114 (1990)
55. Kawai, T., Shimanuki, S.: Optical studies of (CH3NH3) 3Bi2I9 single crystals. Phys. Status Solidi **177**, K43–K45 (1993)
56. Lyu, M., Yun, J.-H., Cai, M., Jiao, Y., Bernhardt, P.V., Zhang, M., Wang, Q., Du, A., Wang, H., Liu, G.: Organic–inorganic bismuth (III)-based material: A lead-free, air-stable and solution-processable light-absorber beyond organolead perovskites. Nano Res. **9**, 692–702 (2016)
57. Li, H., Wu, C., Yan, Y., Chi, B., Pu, J., Li, J., Priya, S.: Fabrication of lead-free (CH3NH3) 3Bi2I9 perovskite photovoltaics in ethanol solvent. Chemsuschem **10**, 3994–3998 (2017)
58. Hebig, J.-C., Kuhn, I., Flohre, J., Kirchartz, T.: Optoelectronic properties of (CH3NH3) 3Sb2I9 thin films for photovoltaic applications. ACS Energy Lett. **1**, 309–314 (2016)
59. Boopathi, K.M., Karuppuswamy, P., Singh, A., Hanmandlu, C., Lin, L., Abbas, S.A., Chang, C.C., Wang, P.C., Li, G., Chu, C.W.: Solution-processable antimony-based light-absorbing materials beyond lead halide perovskites. J. Mater. Chem. A. **5**, 20843–20850 (2017)
60. Ju, M.-G., Dai, J., Ma, L., Zeng, X.C.: Lead-free mixed tin and germanium perovskites for photovoltaic application. J. Am. Chem. Soc. **139**, 8038–8043 (2017)
61. Kopacic, I., Friesenbichler, B., Hoefler, S.F., Kunert, B., Plank, H., Rath, T., Trimmel, G.: Enhanced performance of germanium halide perovskite solar cells through compositional engineering. ACS Appl. Energy Mater. **1**, 343–347 (2018)
62. Cui, X.-P., Jiang, K.-J., Huang, J.-H., Zhang, Q.-Q., Su, M.-J., Yang, L.-M., Song, Y.-L., Zhou, X.-Q.: Cupric bromide hybrid perovskite heterojunction solar cells. Synth. Met. **209**, 247–250 (2015)
63. Li, X., Zhong, X., Hu, Y., Li, B., Sheng, Y., Zhang, Y., Weng, C., Feng, M., Han, H., Wang, J.: Organic–inorganic copper (II)-based material: a low-toxic, highly stable light absorber for photovoltaic application. J. Phys. Chem. Lett. **8**, 1804–1809 (2017)
64. Elseman, A.M., Shalan, A.E., Sajid, S., Rashad, M.M., Hassan, A.M., Li, M.: Copper-substituted lead perovskite materials constructed with different halides for working (CH3NH3)2CuX4-based perovskite solar cells from experimental and theoretical view. ACS Appl. Mater. Interfaces (2018). https://doi.org/10.1021/acsami.8b00495
65. Milot, R.L., Klug, M.T., Davies, C.L., Wang, Z., Kraus, H., Snaith, H.J., Johnston, M.B., Herz, L.M.: The effects of doping density and temperature on the optoelectronic properties of formamidinium tin triiodide thin films. Adv. Mater. **30**, 1804506 (2018)
66. Johnston, M.B., Herz, L.M.: Hybrid perovskites for photovoltaics: charge-carrier recombination, diffusion, and radiative efficiencies. Acc. Chem. Res. **49**, 146–154 (2016)
67. Zhou, Y., Yang, M., Wu, W., Vasiliev, A.L., Zhu, K., Padture, N.P.: Room-temperature crystallization of hybrid-perovskite thin films via solvent–solvent extraction for high-performance solar cells. J. Mater. Chem. A. **3**, 8178–8184 (2015)
68. Stoumpos, C.C., Kanatzidis, M.G.: Halide perovskites: poor Man's high-performance semiconductors. Adv. Mater. **28**, 5778–5793 (2016)
69. Kumar, M.H., Dharani, S., Leong, W.L., Boix, P.P., Prabhakar, R.R., Baikie, T., Shi, C., Ding, H., Ramesh, R., Asta, M., Graetzel, M., Mhaisalkar, S.G., Mathews, N.: Lead-free halide perovskite solar cells with high photocurrents realized through vacancy modulation. Adv. Mater. **26**, 7122–7127 (2014). https://doi.org/10.1002/adma.201401991
70. Stoumpos, C.C., Malliakas, C.D., Kanatzidis, M.G.: Semiconducting tin and lead iodide perovskites with organic cations: phase transitions, high mobilities, and near-infrared photoluminescent properties. Inorg. Chem. **52**, 9019–9038 (2013)
71. Ren, S., Chang, L.-Y., Lim, S.-K., Zhao, J., Smith, M., Zhao, N., V. Bulović, M. Bawendi, S. Gradečak,: Inorganic–organic hybrid solar cell: bridging quantum dots to conjugated polymer nanowires. Nano Lett. **11**, 3998–4002 (2011)
72. Abulikemu, M., Ould-Chikh, S., Miao, X., Alarousu, E., Murali, B., Ndjawa, G.O.N., Barbé, J., El Labban, A., Amassian, A., Del Gobbo, S.: Optoelectronic and photovoltaic properties of the air-stable organohalide semiconductor (CH 3 NH 3) 3 Bi 2 I 9. J. Mater. Chem. A. **4**, 12504–12515 (2016)
73. D. Shi, V. Adinolfi, R. Comin, M. Yuan, E. Alarousu, A. Buin, Y. Chen, S. Hoogland, A. Rothenberger, K. Katsiev, Low trap-state density and long carrier diffusion in organolead trihalide perovskite single crystals, Science (80-.). 347 (2015) 519–522.
74. Ng, C.H., Nishimura, K., Ito, N., Hamada, K., Hirotani, D., Wang, Z., Yang, F., Shen, Q., Yoshino, K., Minemoto, T.: Role of GeI2 and SnF2 additives for SnGe perovskite solar cells. Nano Energy **58**, 130–137 (2019)
75. Ng, C.H., Hamada, K., Kapil, G., Kamarudin, M.A., Wang, Z., Shen, Q., Yoshino, K., Minemoto, T., Hayase, S.: Reducing trap density and carrier concentration by a Ge additive for an efficient quasi 2D/3D perovskite solar cell. J. Mater. Chem. A. **8**, 2962–2968 (2020)

76. Zuo, C., Ding, L.: Lead-free perovskite materials (NH4) 3Sb2IxBr 9–x, Angew. Chemie. **129**, 6628–6632 (2017)
77. Yu, B., Chen, Z., Zhu, Y., Wang, Y., Han, B., Chen, G., Zhang, X., Du, Z., He, Z.: Heterogeneous 2D/3D tin-halides perovskite solar cells with certified conversion efficiency breaking 14%. Adv. Mater. **33**, 2102055 (2021)
78. Leijtens, T., Prasanna, R., Gold-Parker, A., Toney, M.F., McGehee, M.D.: Mechanism of tin oxidation and stabilization by lead substitution in tin halide perovskites. ACS Energy Lett. **2**, 2159–2165 (2017)
79. Hao, F., Stoumpos, C.C., Guo, P., Zhou, N., Marks, T.J., Chang, R.P.H., Kanatzidis, M.G.: Solvent-mediated crystallization of CH3NH3SnI3 films for heterojunction depleted perovskite solar cells. J. Am. Chem. Soc. **137**, 11445–11452 (2015)
80. Shi, T., Zhang, H.-S., Meng, W., Teng, Q., Liu, M., Yang, X., Yan, Y., Yip, H.-L., Zhao, Y.-J.: Effects of organic cations on the defect physics of tin halide perovskites. J. Mater. Chem. A. **5**, 15124–15129 (2017)
81. Boix, P.P., Agarwala, S., Koh, T.M., Mathews, N., Mhaisalkar, S.G.: Perovskite solar cells: beyond methylammonium lead iodide. J. Phys. Chem. Lett. **6**, 898–907 (2015)
82. Wang, Z., Shi, Z., Li, T., Chen, Y., Huang, W.: Stability of perovskite solar cells: a prospective on the substitution of the A cation and X anion. Angew. Chemie Int. Ed. **56**, 1190–1212 (2017)
83. Yang, L., Barrows, A.T., Lidzey, D.G., Wang, T.: Recent progress and challenges of organometal halide perovskite solar cells. Reports Prog. Phys. **79**, 26501 (2016)
84. Zhao, Z., Gu, F., Li, Y., Sun, W., Ye, S., Rao, H., Liu, Z., Bian, Z., Huang, C.: Mixed-organic-cation tin iodide for lead-free perovskite solar cells with an efficiency of 8.12%. Adv. Sci. **4**, 1700204 (2017)
85. Chen, M., Ju, M.-G., Carl, A.D., Zong, Y., Grimm, R.L., Gu, J., Zeng, X.C., Zhou, Y., Padture, N.P.: Cesium titanium (IV) bromide thin films based stable lead-free perovskite solar cells. Joule. **2**, 558–570 (2018)
86. Marshall, K.P., Walker, M., Walton, R.I., Hatton, R.A.: Enhanced stability and efficiency in hole-transport-layer-free CsSnI3 perovskite photovoltaics. Nat. Energy **1**, 16178 (2016). https://doi.org/10.1038/nenergy.2016.178
87. Fang, H.-H., Adjokatse, S., Shao, S., Even, J., Loi, M.A.: Long-lived hot-carrier light emission and large blue shift in formamidinium tin triiodide perovskites. Nat. Commun. **9**, 243 (2018)
88. Zhang, J., Li, S., Yang, P., Liu, W., Liao, Y.: Enhanced stability of lead-free perovskite heterojunction for photovoltaic applications. J. Mater. Sci. **53**, 4378–4386 (2018)
89. I.E. Castelli, J.M. García-Lastra, K.S. Thygesen, K.W. Jacobsen, Bandgap calculations and trends of organometal halide perovskites, APL Mater. 2 (2014).
90. Ran, C., Xi, J., Gao, W., Yuan, F., Lei, T., Jiao, B., Hou, X., Wu, Z.: Bilateral interface engineering toward efficient 2D–3D bulk heterojunction tin halide lead-free perovskite solar cells. ACS Energy Lett. **3**, 713–721 (2018)
91. Laurita, G., Fabini, D.H., Stoumpos, C.C., Kanatzidis, M.G., Seshadri, R.: Chemical tuning of dynamic cation off-centering in the cubic phases of hybrid tin and lead halide perovskites. Chem. Sci. **8**, 5628–5635 (2017)
92. Amat, A., Mosconi, E., Ronca, E., Quarti, C., Umari, P., Nazeeruddin, M.K., Gratzel, M., De Angelis, F.: Cation-induced band-gap tuning in organohalide perovskites: interplay of spin–orbit coupling and octahedra tilting. Nano Lett. **14**, 3608–3616 (2014)
93. Hoefler, S.F., Trimmel, G., Rath, T.: Progress on lead-free metal halide perovskites for photovoltaic applications: a review. Monatshefte Für Chemie-Chemical Mon. **148**, 795–826 (2017)
94. Gupta, S., Bendikov, T., Hodes, G., Cahen, D.: CsSnBr 3, a lead-free halide perovskite for long-term solar cell application: insights on SnF2 addition. ACS Energy Lett. **1**, 1028–1033 (2016)
95. Lee, S.J., Shin, S.S., Kim, Y.C., Kim, D., Ahn, T.K., Noh, J.H., Seo, J., Il Seok, S.: Fabrication of efficient formamidinium tin iodide perovskite solar cells through SnF2–pyrazine complex. J. Am. Chem. Soc. **138**, 3974–3977 (2016)
96. Shao, S., Liu, J., Portale, G., Fang, H., Blake, G.R., ten Brink, G.H., Koster, L.J.A., Loi, M.A.: Highly reproducible Sn-based hybrid perovskite solar cells with 9% efficiency. Adv. Energy Mater. **8**, 1702019 (2018)
97. Liang, L., Gao, P.: Lead-free hybrid perovskite absorbers for viable application: Can we eat the cake and have it too? Adv. Sci. **5**, 1700331 (2018)
98. Ito, N., Kamarudin, M.A., Hirotani, D., Zhang, Y., Shen, Q., Ogomi, Y., Iikubo, S., Minemoto, T., Yoshino, K., Hayase, S.: Mixed Sn–Ge perovskite for enhanced perovskite solar cell performance in air. J. Phys. Chem. Lett. **9**, 1682–1688 (2018)
99. Johansson, M.B., Zhu, H., Johansson, E.M.J.: Extended photoconversion spectrum in low-toxic bismuth halide perovskite solar cells. J. Phys. Chem. Lett. **7**, 3467–3471 (2016). https://doi.org/10.1021/acs.jpclett.6b01452
100. Ma, F., Zhou, M., Jiao, Y., Gao, G., Gu, Y., Bilic, A., Chen, Z., Du, A.: Single layer bismuth iodide: computational exploration of structural, electrical, mechanical and optical properties. Sci. Rep. **5**, 17558 (2015). https://doi.org/10.1038/srep17558
101. Lan, C., Luo, J., Zhao, S., Zhang, C., Liu, W., Hayase, S., Ma, T.: Effect of lead-free (CH3NH3)3Bi2I9 perovskite addition on spectrum absorption and enhanced photovoltaic performance of bismuth triiodide solar cells. J. Alloys Compd. **701**, 834–840 (2017). https://doi.org/10.1016/j.jallcom.2017.01.169
102. Wang, H., Tian, J., Jiang, K., Zhang, Y., Fan, H., Huang, J., Yang, L., Guan, B., Song, Y.: Fabrication of methylammonium bismuth iodide through interdiffusion of solution-processed BiI3/CH3NH3I stacking layers. RSC Adv. **7**, 43826–43830 (2017). https://doi.org/10.1039/C7RA07123J
103. Cortecchia, D., Dewi, H.A., Yin, J., Bruno, A., Chen, S., Baikie, T., Boix, P.P., Grätzel, M., Mhaisalkar, S., Soci, C., Mathews, N.: Lead-free MA2CuClxBr 4–x hybrid perovskites. Inorg. Chem. **55**, 1044–1052 (2016). https://doi.org/10.1021/acs.inorgchem.5b01896
104. Balachandran, N., Robert, T.M., Jayalatha, T., Neema, P.M., Mathew, D., Cyriac, J.: Lead-free, mixed tin-copper perovskites with improved stability and optical properties. J. Alloys Compd. **879**, 160325 (2021). https://doi.org/10.1016/j.jallcom.2021.160325
105. Adonin, S.A., Frolova, L.A., Sokolov, M.N., Shilov, G.V., Korchagin, D.V., Fedin, V.P., Aldoshin, S.M., Stevenson, K.J., Troshin, P.A.: Antimony (V) complex halides: lead-free perovskite-like materials for hybrid solar cells. Adv. Energy Mater. **8**, 1701140 (2018). https://doi.org/10.1002/aenm.201701140
106. Baranwal, A.K., Masutani, H., Sugita, H., Kanda, H., Kanaya, S., Shibayama, N., Sanehira, Y., Ikegami, M., Numata, Y., Yamada, K., Miyasaka, T., Umeyama, T., Imahori, H., Ito, S.: Lead-free perovskite solar cells using Sb and Bi-based A3B2X9 and A3BX6 crystals with normal and inverse cell structures. Nano Converg. **4**, 26 (2017). https://doi.org/10.1186/s40580-017-0120-3
107. Jiang, F., Yang, D., Jiang, Y., Liu, T., Zhao, X., Ming, Y., Luo, B., Qin, F., Fan, J., Han, H., Zhang, L., Zhou, Y.: Chlorine-incorporation-induced formation of the layered phase for antimony-based lead-free perovskite solar cells. J. Am. Chem. Soc. **140**, 1019–1027 (2018). https://doi.org/10.1021/jacs.7b10739
108. Nie, R., Mehta, A., Park, B., Kwon, H.-W., Im, J., Il Seok, S.: Mixed sulfur and iodide-based lead-free perovskite solar cells. J. Am. Chem. Soc. **140**, 872–875 (2018). https://doi.org/10.1021/jacs.7b11332

109. Li, Y.-J., Wu, T., Sun, L., Yang, R.-X., Jiang, L., Cheng, P.-F., Hao, Q.-Q., Wang, T.-J., Lu, R.-F., Deng, W.-Q.: Lead-free and stable antimony–silver-halide double perovskite (CH3NH3)2AgSbI6. RSC Adv. **7**, 35175–35180 (2017). https://doi.org/10.1039/C7RA06130G
110. Karuppuswamy, P., Boopathi, K.M., Mohapatra, A., Chen, H.-C., Wong, K.-T., Wang, P.-C., Chu, C.-W.: Role of a hydrophobic scaffold in controlling the crystallization of methylammonium antimony iodide for efficient lead-free perovskite solar cells. Nano Energy **45**, 330–336 (2018). https://doi.org/10.1016/j.nanoen.2017.12.051
111. Dimesso, L., Das, C., Mayer, T., Jaegermann, W.: Investigation of earth-alkaline (EA= Mg, Ca, Sr) containing methylammonium tin iodide perovskite systems. J. Mater. Sci. **53**, 356–368 (2018)
112. Chu, L.: Pseudohalide anion engineering for highly efficient and stable perovskite solar cells. Matter. **4**, 1762–1764 (2021)
113. Gong, J., Yang, M., Rebollar, D., Rucinski, J., Liveris, Z., Zhu, K., Xu, T.: Divalent anionic doping in perovskite solar cells for enhanced chemical stability. Adv. Mater. **30**, 1800973 (2018). https://doi.org/10.1002/adma.201800973
114. Lee, S.J., Shin, S.S., Im, J., Ahn, T.K., Noh, J.H., Jeon, N.J., Il Seok, S., Seo, J.: Reducing carrier density in formamidinium tin perovskites and its beneficial effects on stability and efficiency of perovskite solar cells. ACS Energy Lett. **3**, 46–53 (2017)
115. Colella, S., Mosconi, E., Fedeli, P., Listorti, A., Gazza, F., Orlandi, F., Ferro, P., Besagni, T., Rizzo, A., Calestani, G.: MAPbI3-xCl x mixed halide perovskite for hybrid solar cells: the role of chloride as dopant on the transport and structural properties. Chem. Mater. **25**, 4613–4618 (2013)
116. Tsai, C., Mohanta, N., Wang, C., Lin, Y., Yang, Y., Wang, C., Hung, C., Diau, E.W.: Formation of stable tin perovskites co-crystallized with three halides for carbon-based mesoscopic lead-free perovskite solar cells. Angew. Chemie Int. Ed. **56**, 13819–13823 (2017)
117. Gu, J., Li, F., Wang, Z., Xie, Y., Yan, L., Zeng, P., Yu, H., Liu, M.: Morphology tuning and its role in optimization of perovskite films fabricated from a novel nonhalide lead source. Adv. Sci. **7**, 2002296 (2020)
118. Jeong, J., Kim, M., Seo, J., Lu, H., Ahlawat, P., Mishra, A., Yang, Y., Hope, M.A., Eickemeyer, F.T., Kim, M.: Pseudo-halide anion engineering for α-FAPbI3 perovskite solar cells. Nature **592**, 381–385 (2021)
119. Rameez, M., Lin, E.Y.-R., Raghunath, P., Narra, S., Song, D., Lin, M.-C., Hung, C.-H., Diau, E.W.-G.: Development of hybrid pseudohalide tin perovskites for highly stable carbon-electrode solar cells. ACS Appl. Mater. Interfaces **12**, 21739–21747 (2020)
120. Wang, C., Zhang, Y., Gu, F., Zhao, Z., Li, H., Jiang, H., Bian, Z., Liu, Z.: Illumination durability and high-efficiency Sn-based perovskite solar cell under coordinated control of phenylhydrazine and halogen ions. Matter. **4**, 709–721 (2021)
121. Li, B., Di, H., Chang, B., Yin, R., Fu, L., Zhang, Y.-N., Yin, L.: Efficient passivation strategy on sn related defects for high performance all-inorganic cssni3 perovskite solar cells. Adv. Funct. Mater. **31**, 2007447 (2021). https://doi.org/10.1002/adfm.202007447
122. Chen, B., Rudd, P.N., Yang, S., Yuan, Y., Huang, J.: Imperfections and their passivation in halide perovskite solar cells. Chem. Soc. Rev. **48**, 3842–3867 (2019). https://doi.org/10.1039/C8CS00853A
123. Kayesh, M.E., Matsuishi, K., Kaneko, R., Kazaoui, S., Lee, J.-J., Noda, T., Islam, A.: Coadditive engineering with 5-ammonium valeric acid iodide for efficient and stable Sn perovskite solar cells. ACS Energy Lett. **4**, 278–284 (2018)
124. Wang, T., Tai, Q., Guo, X., Cao, J., Liu, C.K., Wang, N., Shen, D., Zhu, Y., Lee, C.S., Yan, F.: Highly air-stable tin-based perovskite solar cells through grain-surface protection by gallic acid. ACS Energy Lett. **5**, 1741–1749 (2020)
125. Tai, Q., Guo, X., Tang, G., You, P., Ng, T., Shen, D., Cao, J., Liu, C., Wang, N., Zhu, Y.: Antioxidant grain passivation for air-stable tin-based perovskite solar cells. Angew. Chemie Int. Ed. **58**, 806–810 (2019)
126. Ye, T., Wang, K., Hou, Y., Yang, D., Smith, N., Magill, B., Yoon, J., Mudiyanselage, R.R.H.H., Khodaparast, G.A., Wang, K., Priya, S.: Ambient-air-stable lead-free cssni3 solar cells with greater than 7.5% efficiency. J. Am. Chem. Soc. **143**, 4319–4328 (2021). https://doi.org/10.1021/jacs.0c13069
127. Zeng, W., Cui, D., Li, Z., Tang, Y., Yu, X., Li, Y., Deng, Y., Ye, R., Niu, Q., Xia, R.: Surface optimization by poly (α-methylstyrene) as additive in the antisolution to enhance lead-free Sn-based perovskite solar cells. Sol. Energy **194**, 272–278 (2019)
128. Liu, G., Liu, C., Lin, Z., Yang, J., Huang, Z., Tan, L., Chen, Y.: Regulated crystallization of efficient and stable tin-based perovskite solar cells via a self-sealing polymer. ACS Appl. Mater. Interfaces **12**, 14049–14056 (2020)
129. Ran, C., Wu, Z., Xi, J., Yuan, F., Dong, H., Lei, T., He, X., Hou, X.: Construction of compact methylammonium bismuth iodide film promoting lead-free inverted planar heterojunction organohalide solar cells with open-circuit voltage over 08 V. J. Phys. Chem. Lett. **8**, 394–400 (2017)
130. Zhang, Z., Li, X., Xia, X., Wang, Z., Huang, Z., Lei, B., Gao, Y.: High-quality (CH3NH3) 3Bi2I9 film-based solar cells: pushing efficiency up to 1.64%. J. Phys. Chem. Lett. **8**, 4300–4307 (2017)
131. Liao, W., Zhao, D., Yu, Y., Grice, C.R., Wang, C., Cimaroli, A.J., Schulz, P., Meng, W., Zhu, K., Xiong, R.: Lead-free inverted planar formamidinium tin triiodide perovskite solar cells achieving power conversion efficiencies up to 6.22%. Adv. Mater. **28**, 9333–9340 (2016)
132. Ran, C., Gao, W., Li, J., Xi, J., Li, L., Dai, J., Yang, Y., Gao, X., Dong, H., Jiao, B.: Conjugated organic cations enable efficient self-healing FASnI3 solar cells. Joule. **3**, 3072–3087 (2019)
133. Wu, T., Liu, X., He, X., Wang, Y., Meng, X., Noda, T., Yang, X., Han, L.: Efficient and stable tin-based perovskite solar cells by introducing π-conjugated Lewis base. Sci. China Chem. **63**, 107–115 (2020)
134. Ke, W., Priyanka, P., Vegiraju, S., Stoumpos, C.C., Spanopoulos, I., Soe, C.M.M., Marks, T.J., Chen, M.-C., Kanatzidis, M.G.: Dopant-free tetrakis-triphenylamine hole transporting material for efficient tin-based perovskite solar cells. J. Am. Chem. Soc. **140**, 388–393 (2018)
135. Vegiraju, S., Ke, W., Priyanka, P., Ni, J., Wu, Y., Spanopoulos, I., Yau, S.L., Marks, T.J., Chen, M., Kanatzidis, M.G.: Benzodithiophene hole-transporting materials for efficient tin-based perovskite solar cells. Adv. Funct. Mater. **29**, 1905393 (2019)
136. Zhu, Z., Chueh, C., Li, N., Mao, C., Jen, A.K.: Realizing efficient lead-free formamidinium tin triiodide perovskite solar cells via a sequential deposition route. Adv. Mater. **30**, 1703800 (2018)
137. Meng, X., Wu, T., Liu, X., He, X., Noda, T., Wang, Y., Segawa, H., Han, L.: Highly reproducible and efficient FASnI3 perovskite solar cells fabricated with volatilizable reducing solvent. J. Phys. Chem. Lett. **11**, 2965–2971 (2020)
138. Meng, X., Wang, Y., Lin, J., Liu, X., He, X., Barbaud, J., Wu, T., Noda, T., Yang, X., Han, L.: Surface-controlled oriented growth of FASnI3 crystals for efficient lead-free perovskite solar cells. Joule. **4**, 902–912 (2020). https://doi.org/10.1016/j.joule.2020.03.007
139. Wang, C., Gu, F., Zhao, Z., Rao, H., Qiu, Y., Cai, Z., Zhan, G., Li, X., Sun, B., Yu, X.: Self-repairing tin-based perovskite solar cells with a breakthrough efficiency over 11%. Adv. Mater. **32**, 1907623 (2020)

140. Liu, X., Wu, T., Chen, J.-Y., Meng, X., He, X., Noda, T., Chen, H., Yang, X., Segawa, H., Wang, Y.: Templated growth of FASnI 3 crystals for efficient tin perovskite solar cells. Energy Environ. Sci. **13**, 2896–2902 (2020)
141. Cui, D., Liu, X., Wu, T., Lin, X., Luo, X., Wu, Y., Segawa, H., Yang, X., Zhang, Y., Wang, Y.: Making room for growing oriented FASnI3 with large grains via cold precursor solution. Adv. Funct. Mater. **31**, 2100931 (2021)
142. Wang, T., Zheng, F., Tang, G., Cao, J., You, P., Zhao, J., Yan, F.: 2D WSe2 flakes for synergistic modulation of grain growth and charge transfer in tin-based perovskite solar cells. Adv. Sci. **8**, 2004315 (2021)
143. Kim, H., Lee, Y.H., Lyu, T., Yoo, J.H., Park, T., Oh, J.H.: Boosting the performance and stability of quasi-two-dimensional tin-based perovskite solar cells using the formamidinium thiocyanate additive. J. Mater. Chem. A. **6**, 18173–18182 (2018)
144. Wang, F., Jiang, X., Chen, H., Shang, Y., Liu, H., Wei, J., Zhou, W., He, H., Liu, W., Ning, Z.: 2D-quasi-2D-3D hierarchy structure for tin perovskite solar cells with enhanced efficiency and stability. Joule. **2**, 2732–2743 (2018)
145. Jokar, E., Chien, C., Tsai, C., Fathi, A., Diau, E.W.: Robust tin-based perovskite solar cells with hybrid organic cations to attain efficiency approaching 10%. Adv. Mater. **31**, 1804835 (2019)
146. Shao, S., Dong, J., Duim, H., ten Brink, G.H., Blake, G.R., Portale, G., Loi, M.A.: Enhancing the crystallinity and perfecting the orientation of formamidinium tin iodide for highly efficient Sn-based perovskite solar cells. Nano Energy **60**, 810–816 (2019)
147. Qiu, J., Xia, Y., Zheng, Y., Hui, W., Gu, H., Yuan, W., Yu, H., Chao, L., Niu, T., Yang, Y.: 2D intermediate suppression for efficient ruddlesden-popper (RP) phase lead-free perovskite solar cells. ACS Energy Lett. **4**(7), 1513–1520 (2019)
148. Li, P., Liu, X., Zhang, Y., Liang, C., Chen, G., Li, F., Su, M., Xing, G., Tao, X., Song, Y.: Low-dimensional dion–jacobson-phase lead-free perovskites for high-performance photovoltaics with improved stability. Angew. Chemie Int. Ed. **59**, 6909–6914 (2020)
149. Nishimura, K., Kamarudin, M.A., Hirotani, D., Hamada, K., Shen, Q., Iikubo, S., Minemoto, T., Yoshino, K., Hayase, S.: Lead-free tin-halide perovskite solar cells with 13% efficiency. Nano Energy **74**, 104858 (2020)
150. Nakamura, T., Yakumaru, S., Truong, M.A., Kim, K., Liu, J., Hu, S., Otsuka, K., Hashimoto, R., Murdey, R., Sasamori, T.: Sn (IV)-free tin perovskite films realized by in situ Sn (0) nanoparticle treatment of the precursor solution. Nat. Commun. **11**, 1–8 (2020)
151. Jokar, E., Cheng, P.-Y., Lin, C.-Y., Narra, S., Shahbazi, S., Wei-Guang Diau, E.: Enhanced performance and stability of 3D/2D tin perovskite solar cells fabricated with a sequential solution deposition. ACS Energy Lett. **6**, 485–492 (2021)
152. Chen, Y., Cao, K., Cheng, Y., Shen, H., Du, C., Wang, Q., Chen, C., Cui, H., Lan, T., Liu, L.: p-Type dopants as dual function interfacial layer for efficient and stable tin perovskite solar cells. Sol. RRL. **5**, 2100068 (2021)
153. Ding, D., Lanzetta, L., Liang, X., Min, G., Giza, M., Macdonald, T.J., Haque, S.A.: Ultrathin polymethylmethacrylate interlayers boost performance of hybrid tin halide perovskite solar cells. Chem. Commun. **57**, 5047–5050 (2021)
154. Jiang, X., Li, H., Zhou, Q., Wei, Q., Wei, M., Jiang, L., Wang, Z., Peng, Z., Wang, F., Zang, Z.: One-step synthesis of SnI2·(DMSO) x adducts for high-performance tin perovskite solar cells. J. Am. Chem. Soc. **143**, 10970–10976 (2021)
155. Liu, G., Zhong, Y., Feng, W., Yang, M., Yang, G., Zhong, J.-X., Tian, T., Luo, J.-B., Tao, J., Yang, S., Wang, X.-D., Tan, L., Chen, Y., Wu, W.-Q.: Multidentate chelation heals structural imperfections for minimized recombination loss in lead-free perovskite solar cells. Angew. Chemie Int. Ed. **61**, e202209464 (2022). https://doi.org/10.1002/anie.202209464
156. Liu, G., Jiang, X., Feng, W., Yang, G., Chen, X., Ning, Z., Wu, W.-Q.: Synergic electron and defect compensation minimizes voltage loss in lead-free perovskite solar cells. Angew. Chemie Int. Ed. **62**, e202305551 (2023). https://doi.org/10.1002/anie.202305551
157. Park, B.-W., Philippe, B., Zhang, X., Rensmo, H., Boschloo, G., Johansson, E.M.J.: Bismuth based hybrid perovskites A3Bi2I9 (A: Methylammonium or Cesium) for solar cell application. Adv. Mater. **27**, 6806–6813 (2015). https://doi.org/10.1002/adma.201501978
158. Jain, S.M., Edvinsson, T., Durrant, J.R.: Green fabrication of stable lead-free bismuth based perovskite solar cells using a non-toxic solvent. Commun. Chem. **2**, 91 (2019)
159. Li, J., Liu, X., Xu, J., Chen, J., Zhao, C., Salma Maneno, M., Zhang, B., Yao, J.: Fabrication of sulfur-incorporated bismuth-based perovskite solar cells via a vapor-assisted solution process. Sol. RRL. **3**, 1900218 (2019)
160. M.I. Khan, A. Mukhtar, N. Alwadai, M. Irfan, I. Haq, H. Albalawi, A.H. Almuqrin, M.M. Almoneef, M. Iqbal, Improving the Structural, Optical and Photovoltaic Properties of Sb- and Bi-Co-Doped MAPbBr3 Perovskite Solar Cell, Coatings. 12 (2022). https://doi.org/10.3390/coatings12030386.
161. Chatterjee, S., Pal, A.J.: Tin (IV) substitution in (CH3NH3) 3Sb2I9: toward low-band-gap defect-ordered hybrid perovskite solar cells. ACS Appl. Mater. Interfaces **10**, 35194–35205 (2018)
162. Zhu, Z., Jiang, X., Yu, D., Yu, N., Ning, Z., Mi, Q.: Smooth and compact FASnI3 films for lead-free perovskite solar cells with over 14% efficiency. ACS Energy Lett. **7**, 2079–2083 (2022)